PLOS COMPUTATIONAL BIOLOGY

RESEARCH ARTICLE

Amplifying the redistribution of somato-dendritic inhibition by the interplay of three interneuron types

Loreen Hertäg[1,2]*, **Henning Sprekeler**[1,2]*

1 Modelling of Cognitive Processes, Berlin Institute of Technology, Berlin, Germany, **2** Bernstein Center for Computational Neuroscience, Berlin, Germany

* loreen.hertaeg@tu-berlin.de (LH); h.sprekeler@tu-berlin.de (HS)

OPEN ACCESS

Citation: Hertäg L, Sprekeler H (2019) Amplifying the redistribution of somato-dendritic inhibition by the interplay of three interneuron types. PLoS Comput Biol 15(5): e1006999. https://doi.org/10.1371/journal.pcbi.1006999

Editor: Hermann Cuntz, Goethe University, GERMANY

Received: December 18, 2018

Accepted: April 1, 2019

Published: May 16, 2019

Data Availability Statement: All relevant data are within the manuscript and its Supporting Information files.

Funding: This work was funded by the German Federal Ministry for Education and Research, FKZ 01GQ1201. The funders had no role in study design, data collection and analysis, decision to publish, or preparation of the manuscript.

Competing interests: The authors have declared that no competing interests exist.

Abstract

GABAergic interneurons play an important role in shaping the activity of excitatory pyramidal cells (PCs). How the various inhibitory cell types contribute to neuronal information processing, however, is not resolved. Here, we propose a functional role for a widespread network motif consisting of parvalbumin- (PV), somatostatin- (SOM) and vasoactive intestinal peptide (VIP)-expressing interneurons. Following the idea that PV and SOM interneurons control the distribution of somatic and dendritic inhibition onto PCs, we suggest that mutual inhibition between VIP and SOM cells translates weak inputs to VIP interneurons into large changes of somato-dendritic inhibition of PCs. Using a computational model, we show that the neuronal and synaptic properties of the circuit support this hypothesis. Moreover, we demonstrate that the SOM-VIP motif allows transient inputs to persistently switch the circuit between two processing modes, in which top-down inputs onto apical dendrites of PCs are either integrated or cancelled.

Author summary

Neurons in the brain can be classified as excitatory or inhibitory based on whether they activate or deactivate the cells to whom they send signals. Compared to their excitatory counterpart, inhibitory neurons present themselves as a wild diversity of cell classes. It is broadly believed that these classes serve different purposes, but as of now, those are poorly understood. In this article, we suggest how an intricate interplay of three inhibitory cell classes can control whether internal signals—such as predictions, memory signals or motor commands—are taken into account when sensory signals are interpreted. Using a mathematical model and computer simulations, we show that such internal signals can be shut down by regulating which inhibitory cell types are active, and that the interaction of different cell classes allows weak control signals to do so.

Introduction

GABAergic interneurons are essential for maintaining normal brain activity [1–3], although they are outnumbered by excitatory cells throughout the brain [4]. They present a large number of distinct types that differ in their anatomical, physiological and biophysical properties [3, 5, 6]. This has led to the hypothesis that individual types are optimized to perform specific computations in neuronal microcircuits [3, 7–10]. The functional roles of these interneuron classes and how they are supported by their individual characteristics, however, are still largely unknown.

One conspicuous difference between interneuron types is the location of their synapses onto their postsynaptic targets: Parvalbumin-expressing (PV) interneurons preferably inhibit the perisomatic regions and the basal dendrites of excitatory pyramidal cells (PCs), as well as other PV neurons [3, 11–15]. In contrast, somatostatin-expressing (SOM) neurons mainly target the apical dendrites of PCs, and strongly inhibit other interneuron types [13, 15, 16]. A third group expressing vasoactive intestinal peptide (VIP) mainly connects to the dendrite-targeting SOM neurons, thereby providing a disinhibitory circuit for the distal dendrite of PCs [13, 17–20]. In addition to these distinct connectivity motifs, different interneuron types also differ in their intrinsic and synaptic properties. For instance, PV neurons hardly exhibit spike-frequency adaptation [3, 11, 14], a neuronal characteristic that has been observed both for SOM [3, 16] and VIP cells [3].

As a consequence of the interneuron-specific, spatially distinct distribution of synapses onto PCs and the direct connection from SOM to PV neurons, it has been hypothesized that the SOM-PV motif plays a key role in the redistribution of somatic and dendritic inhibition [13, 21]. Inhibiting specific compartments of PCs may have wide-ranging functional and computational consequences, because their somata and dendrites are the target of two distinct information streams. Top-down input originating from higher cortical areas and non-specific thalamocortical pathways [22–24] selectively aims at apical dendrites [25]. At the same time, feedforward bottom-up input from lower cortical areas and the core thalamic nuclei arrives at perisomatic regions and basal dendrites [25]. While top-down feedback is associated with internal predictions, bottom-up connections are thought to carry information from the external world [25]. Hence, control of the different input streams—and consequently, information processing modes—is of fundamental importance.

Here, we hypothesize that a different subnetwork consisting of SOM and VIP neurons is optimized to efficiently control the PV/SOM-mediated redistribution of somatic and dendritic inhibition. In order to support our hypothesis, we perform mathematical analyses and extensive simulations of a microcircuit consisting of these three interneuron types and excitatory PCs. We show that mutual inhibition between VIP and SOM neurons (that is, VIP neurons inhibit SOM neurons and vice versa) leads to an amplification of weak signals targeting VIP neurons. When this mutual inhibition is strong, it can even turn the SOM-VIP motif into a winner-take-all (WTA) circuit. Furthermore, we reveal how frequently reported connectivity, neuronal and synaptic properties underpin the amplification abilities of the microcircuit, such as the lack of recurrent connections among both SOM and VIP cells, their prominent spike-frequency adaptation and short-term facilitation. Moreover, we show that the circuit can display slow oscillations ranging from Delta to Alpha bands as a consequence of spike-frequency adaptation and strong mutual inhibition in SOM and VIP neurons.

Functionally, strong mutual inhibition between SOM and VIP neurons enables a switch between two distinct processing modes in which top-down inputs arriving at the apical dendrites of PCs are either integrated or obliterated via VIP cell modulation. The transition

between these operating modes can be triggered by either weak and persistent input or strong and transient pulses.

Results

We study a rate-based network model consisting of excitatory PC and inhibitory PV, SOM and VIP cells (see Fig 1A). The ratio of excitatory and inhibitory neurons and the strength and probability of their connections are constrained by experimental findings [12, 13, 15, 17, 26–32] (see Tables 1–3). While GABAergic neurons are described by point neuron models [33], PCs are modeled as two compartments, to capture both somatic activity and active processes in their apical dendrites [34] (see Methods).

All neurons receive background input to ensure similar firing rates as observed *in vivo* [5, 16, 31]. PC input is divided into two separate information streams: top-down feedback arriving at the apical dendrite and bottom-up input targeting the perisomatic region. In addition, we consider modulatory inputs onto VIP and SOM cells that regulate the distribution of somatic and dendritic inhibition. This modulation could be mediated by, e.g., excitatory long-range

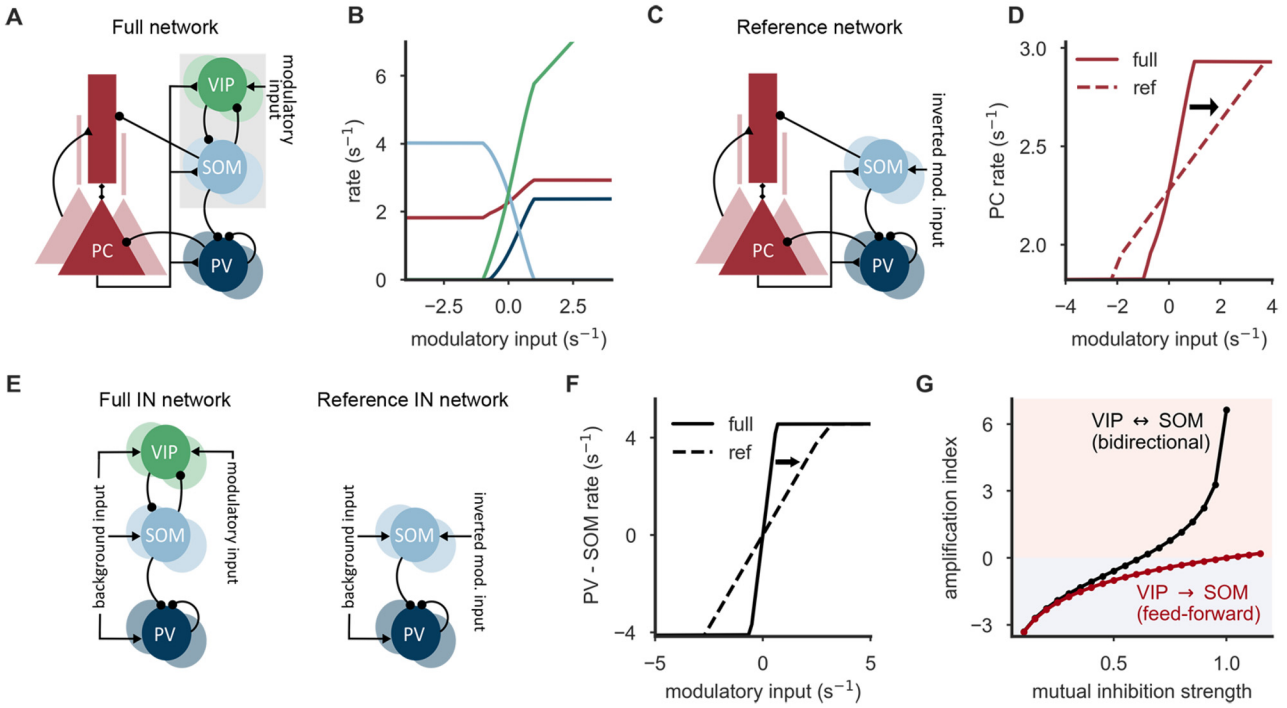

Fig 1. Amplifying the redistribution of inhibition along PCs by the SOM-VIP motif. (A) Connectivity of the circuit model, inspired by experimentally observed connectivity of excitatory pyramidal cells (PCs) and inhibitory PV, SOM and VIP neurons (see main text). VIP neurons receive an additional, modulatory input. **(B)** Population rates of all neuron types as a function of the modulatory input onto VIP cells. The PC rate follows a sigmoid function, the slope of which characterizes the gain of the redistribution of somato-dendritic inhibition upon a change in the modulatory input. **(C)** Reference network without VIP neurons, in which modulatory input targets SOM neurons instead (with inverted sign for comparability). **(D)** The firing rate curve of the PCs in the full network (A) exhibit a larger slope than in the reference network without VIP neurons (C). Reference curve shifted for comparability. **(E)** Reduced network of inhibitory PV, SOM and VIP neurons (left) that allows a mathematical analysis, and a corresponding reference network without VIP neurons (right). **(F)** The difference of PV and SOM neuron rates (somatic and dendritic inhibition, respectively) follows a sigmoid function. In the full interneuron network (E, left), it exhibits a larger slope than a corresponding reference network without VIP neurons (E, right) (mutual inhibition strength $\hat{w} = 0.9$). **(G)** Amplification index depends strongly on the mutual inhibition strength. Positive values denote an amplification, negative values indicate an attenuation. An infinitely large amplification index corresponds to a winner-take-all (WTA) regime. When the connections from SOM to VIP neurons are knocked-out (red), the amplification index rises slowly—logarithmically with the connection from VIP to SOM neurons—and reaches the amplification regime for much larger connection strengths. Parameters (A-D): Mutual inhibition strength $\hat{w} = 0.7$, adaptation strength $b = 0.2$, initial synaptic efficacy $U_s = 0.4$.

https://doi.org/10.1371/journal.pcbi.1006999.g001

Table 1. Connection probabilities between neuron types. Entries in the same columns correspond to the same presynaptic neuron type, entries in the same row to the same postsynaptic neuron type. Parentheses denote values that are only used when recurrence is introduced artificially. E: somatic PC compartment, D: dendritic PC compartment.

		pre:			
		E (PC som.)	**PV**	**SOM**	**VIP**
post:	**E (PC som.)**	-	0.6	-	-
	D (PC dendr.)	0.1	-	0.55	-
	PV	0.45	0.5	0.6	-
	SOM	0.35	-	(0.5)	0.5
	VIP	0.1	-	0.45	(0.5)

https://doi.org/10.1371/journal.pcbi.1006999.t001

Table 2. PC parameters describing the two-compartment rate model. $\hat{w}_{EP}$, $\hat{w}_{DS}$ and $\hat{w}_{DE}$ denote the total strength of connection between PV neurons and the soma of PCs, SOM neurons and the dendrites of PCs and the recurrence strength between PCs, respectively. The total connection strength is given by the product of the number of existing connections between two neuron types (or compartments) and the strength for individual connections. All parameters taken from Murayama et al. (2009) [34]. Note that we incorporated the gain factor present in Murayama et al. (2009) [34] into the parameters to achieve unit consistency for all neuron types.

parameter (unit)	value
Θ (s^{-1})	14
λ_E	0.31
λ_D	0.27
$\hat{w}_{EP}$	0.7
$\hat{w}_{DS}$	1.96
$\hat{w}_{DE}$	0.42
c (s^{-1})	7
Θ_c (s^{-1})	28

https://doi.org/10.1371/journal.pcbi.1006999.t002

inputs [18, 19, 29] or by neuromodulatory signals [18, 35–38]. Because inputs to SOM and VIP cells have antagonistic effects in the circuit, we simplified the analysis by considering a single modulatory input to VIP cells, which can be interpreted as a weighted difference between two separate modulatory inputs to SOM and VIP neurons. For example, a strong inhibitory modulation of VIP neurons would be functionally equivalent to a strong excitatory input to SOM neurons that in turn mediates an inhibition of the VIP neurons.

The distribution of somatic and dendritic inhibition onto PCs is regulated by VIP input as follows (see Fig 1B): When the modulatory VIP input is sufficiently small or even inhibitory,

Table 3. Connection strengths between neuron types. Entries in the same columns correspond to the same presynaptic neuron type, entries in the same row to the same postsynaptic neuron type. Given are the total connection strengths (absolute values, sign in simulations in line with neuron type—excitatory/inhibitory), which are the product of the number of existing connections between two neuron types (or compartments) and the strength for individual connections. The total recurrence strengths $\hat{w}_{SS}$ and $\hat{w}_{VV}$ as well as the total mutual inhibition strengths $\hat{w}_{SV}$ and $\hat{w}_{VS}$ are varied in the simulations. Parentheses denote values that are only used when recurrence is introduced artificially.

		pre:			
		E	**PV**	**SOM**	**VIP**
post:	**PV**	1	1.5	1.3	-
	SOM	1	-	$(\hat{w}_{SS})$	$\hat{w}_{SV}$
	VIP	1	-	$\hat{w}_{VS}$	$(\hat{w}_{VV})$

https://doi.org/10.1371/journal.pcbi.1006999.t003

VIP neurons remain inactive. As this relieves the SOM neurons from VIP inhibition, they can in turn inhibit the apical dendrites of the PCs and thereby suppress potential top-down inputs. At the same time, the amount of somatic inhibition in PCs is reduced, because SOM cells inhibit PV neurons. Once VIP cells are fully deactivated, further reducing the modulatory input has no effect on the PCs, as the modulatory input acts through VIP neurons only (Fig 1A). The opposite scenario is a strong and excitatory modulatory input that renders VIP cells sufficiently active to silence SOM neurons. Silencing SOM cells removes dendritic inhibition, so that PCs are receptive to both bottom-up input and top-down feedback. In turn, the perisomatic compartments of PCs experience more inhibition, because PV neurons are released from SOM neuron inhibition. Once the VIP cells are sufficiently active to silence SOM neurons, further increasing the modulatory input has no effect on the PCs, because VIP cells act through SOM neurons only (Fig 1A). VIP neurons then effectively decouple from the microcircuit. In between these two extremes of inactive VIP or SOM neurons, respectively, the ratio of somatic and dendritic inhibition can be controlled by adjusting the modulatory signal. This is reflected by the relationship between modulatory VIP input and PC activity, which resembles a sigmoid function (Fig 1B), the slope of which characterizes the gain of the redistribution of somatic and dendritic inhibition upon a change in the modulatory input. Please note that a redistribution of inhibition from the dendrites to the soma can either increase or decrease the activity of the PCs depending on the parameters of the model, but this does not affect the results presented in the following.

In principle, a similar somato-dendritic redistribution of inhibition could also be achieved by modulatory input directly to SOM neurons. To understand the role of the SOM-VIP motif in the circuit, we considered a 'reference network' without VIP neurons (Fig 1C), in which the modulatory input targets SOM cells instead (with inverted sign for comparability). We found that in this reference network, the slope of the corresponding sigmoid function decreases (Fig 1D) for a large parameter range, indicating that inputs onto VIP neurons in the SOM-VIP motif are more effective modulators than inputs onto SOM neurons. This observation led us to the hypothesis that the SOM-VIP motif serves to translate weak signals onto VIP neurons into large changes of the somato-dendritic distribution of inhibition. We therefore wondered whether the connectivity and the neuronal and synaptic properties of the circuit are optimized to support this function, and which computational purpose the circuit could fulfill. To address these questions, computational modeling is well suited, because it allows us to study the effect of arbitrary manipulations and variations of the circuit.

Mutual inhibition between SOM and VIP neurons creates an amplifier

To gain a deeper understanding of the circuit mechanisms and the interplay of the interneuron types, we next studied a simplified microcircuit consisting only of the three interneuron classes expressing PV, SOM and VIP (Fig 1E, left). The advantage of this simpler model is that it bypasses the nonlinearities of PCs, thereby allowing an in-depth mathematical analysis of the parameter dependencies of the network. All results are later verified in the full circuit. In the simplified network, the local PC input onto the GABAergic interneurons is replaced by additional excitatory inputs to maintain realistic firing rates. Compartment-specific inhibition onto PCs is represented by the population firing rate of the respective interneuron type: the rate of SOM neurons reflects the strength of dendritic inhibition and the rate of PV neurons the strength of somatic inhibition. Similar to the PC rate in the full microcircuit, the difference of the PV and SOM neuron rates shows a sigmoidal dependence on the modulatory VIP cell input (Fig 1F), the slope of which quantifies the system's sensitivity to changes in the modulatory input.

Again, we compared the circuit to a reference network without VIP neurons (Fig 1E, right), in which modulatory inputs impinged directly onto the SOM neurons. In line with the full model, we observed that the removal of the VIP neurons led to a prominent reduction of the sensitivity to modulatory inputs, i.e., a reduced slope of the somato-dendritic difference of inhibition (cf. Fig 1D and 1F). To quantify the effect of the SOM-VIP motif, we introduced an *amplification index A*, defined as the logarithm of the ratio of slopes in the two networks with and without VIP neurons (cf. Fig 1F solid and dashed lines, and see Methods for more details). An amplification index larger than zero indicates that the interneuron network amplifies weak input onto VIP neurons in comparison to the reference network.

The simplified circuit allows us to derive a mathematical expression for the amplification index, which shows that the amount of amplification depends critically on two circuit properties (see Methods for a detailed derivation). Firstly, it increases with the effective VIP→SOM connection strength, reflecting the monosynaptic effect of VIP inputs onto SOM neurons. Secondly, it depends in a highly nonlinear way on the product of the connection strengths from SOM→VIP and VIP→SOM. This second dependence is a consequence of the mutual inhibition between SOM and VIP neurons: an increase in VIP firing rate not only inhibits SOM neurons, but also further disinhibits the VIP neurons themselves, which in turn increase their rate, further inhibiting the SOM neurons etc. As this mutual inhibition approaches a critical strength, the amplification index increases rapidly. Beyond the critical strength, the circuit transitions into a competitive winner-take-all regime, in which either the SOM or the VIP neurons are silenced by the other population. Our mathematical analysis is confirmed by simulations, which also show a rapid increase of the amplification index as the mutual inhibition between VIP and SOM neurons increases (see Fig 1G for symmetric mutual inhibition strengths, and S1 Fig for asymmetric weights). Much stronger VIP→SOM connection strengths are required to achieve an amplification ($A > 0$) when the back-projection SOM→VIP is knocked out, effectively eliminating the mutual competition between VIP and SOM neurons (red line in Fig 1G). These results demonstrate that mutual inhibition is a key player in the amplification of weak inputs onto VIP cells.

Connectivity and short-term plasticity support the amplification

If the SOM-VIP motif were to serve as an amplifier for weak modulatory signals, other circuit properties should also support this function. A candidate mechanism that would further enhance the competition between SOM and VIP is synaptic short-term faciliation (STF). Although short-term plasticity between different types of GABAergic interneurons has received limited attention, STF has indeed been demonstrated for the mutual connections between SOM and VIP neurons [39]. We therefore enhanced the network model by a Tsodyks-Markram type model of short-term plasticity [40, 41] (see Methods for more details). For the sake of simplicity, SOM→VIP and VIP→SOM synapses had equal facilitation parameters (Fig 2A). The overall STF strength was varied by changing the initial release probability, while adjusting the synaptic weight in order to keep the initial postsynaptic response constant (see Methods for further details). As expected, STF causes an increase of the amplification index, such that smaller mutual inhibition strengths are sufficient to achieve an amplification index above the amplification threshold $A = 0$ (Fig 2A).

In contrast to PV neurons, which show strong inhibitory connections onto other PV cells [3, 13, 14], SOM and VIP neurons only very rarely inhibit other neurons of the same class [3, 13, 15]. To investigate whether this lack of recurrent inhibition supports the amplification properties of the network, we artificially introduced recurrent connections among both SOM and VIP neurons. We systematically varied their strength, while keeping the strength of

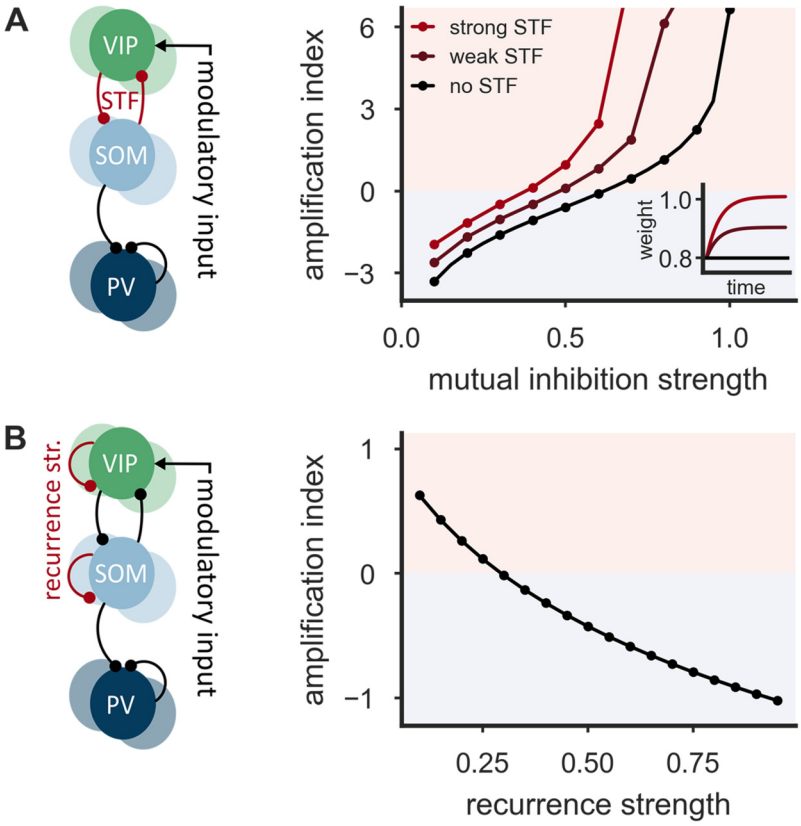

Fig 2. Connectivity properties of the SOM-VIP motif support the amplification in the interneuron network. (A) Network of inhibitory PV, SOM and VIP neurons with short-term facilitation (STF) of SOM→VIP and VIP→SOM connections (left). STF increases the amplification index. Smaller mutual inhibition strengths are sufficient to achieve an amplification index above the amplification threshold $A = 0$ (right). Inset: The dynamics of the mutual inhibition strength ('weight') after a step increase of the presynaptic firing rate from 0/s to 5/s for three different values of the initial release probabilities. STF parameters are equal for SOM and VIP neurons: $U_s = 0.1$ (strong STF), $U_s = 0.5$ (weak STF), $U_s = 1$ (no STF) and $\tau_f = 100$ ms. **(B)** Network of inhibitory PV, SOM and VIP neurons with artificially introduced recurrent connections among both SOM and VIP neurons (left). Recurrence leads to a decrease of the amplification index (right). Recurrence strengths are equal for SOM and VIP neurons. Mutual inhibition strength $\hat{w} = 0.8$.

https://doi.org/10.1371/journal.pcbi.1006999.g002

mutual inhibition between the two populations constant. For simplicity, we considered a symmetric situation in which the strength of the recurrent inhibition is the same among VIP and SOM neurons (see Fig 2B), but similar results are obtained in asymmetric situations (see S2 Fig). We found that recurrent connections among SOM and VIP neurons lead to a strong reduction of the amplification index (Fig 2B), even for relatively weak recurrent connections (see Methods for a mathematical analysis). The strongest amplification was always observed for a connection strength of zero, that is, when recurrent inhibition is absent.

In summary, connectivity properties like short-term facilitation and the absence of recurrent connections among both VIP and SOM neurons support the effective translation of small stimuli onto VIP cells into large changes of somato-dendritic inhibition.

Spike-frequency adaptation introduces a frequency-selective amplification

Both SOM and VIP neurons show an absence of recurrent inhibition within the same population, but they make use of a different negative feedback mechanism: spike-frequency adaptation (SFA). SFA is a prominent feature observed in many cortical neurons [3, 42]. Upon

stimulation, adapting cells decrease their firing rate gradually, and consequently exhibit a difference between steady-state and onset firing rate. SOM neurons feature salient SFA [3, 5, 6, 11, 16], whereas VIP neurons claim a broad spectrum from weak to strong adaptation. To study the effect of SFA, we augmented the rate dynamics of SOM and VIP neurons by an additional rate adaptation variable (see Methods). The adaptation process is governed by two parameters: an adaptation strength and a time constant. While the adaptation time constant controls the temporal evolution of the adaptation process, the adaptation strength controls the difference between onset and steady-state firing rate. An adaptation strength of one corresponds to a steady-state firing rate that is half the onset firing rate. For simplicity, we again assumed the same adaptation parameters for SOM and VIP neurons.

Adaptation and recurrence both generate a negative feedback on neuronal activity. For comparability, we parameterized the strength of recurrence such that the steady state activity in a population is the same when adaptation strength and total recurrence strength have the same value. While we expected both adaptation and recurrent inhibition to weaken the amplification, they differ with respect to the time scales on which they operate. Recurrent inhibition acts on the rapid time scale of synaptic transmission (e.g, of 5–10 ms for $GABA_A$ receptor-based transmission). In contrast, adaptation operates on a wide range of time scales from tens to thousands of milliseconds [42]. Consequently, adaptation allows a gradual transition over time from amplification to attenuation. To characterize the time dependence of the amplification properties, we performed a frequency response analysis (Fig 3A and 3B), a common technique to analyze linear dynamical systems. The idea is that any input signal can be decomposed into oscillations of different frequencies, and that the system processes these different oscillations independently. In practice, this means that the response of the system to any signal can be understood as a superposition of the responses to its frequency components. To characterize the response of the circuit to different frequencies, we hence stimulated VIP neurons with oscillating inputs. The difference of the population firing rates of PV and SOM neurons—as a reflection of the somato-dendritic distribution of inhibition—oscillates in response to this stimulation with the same frequency, but phase-shifted. The logarithm of the ratio of the oscillation amplitudes in networks with and without VIP neurons (full vs. reference network, see Fig 1) yields a frequency-resolved amplification index that ranges from negative (attenuation) to positive (amplification) values. We found that increasing recurrent inhibition among both SOM and VIP neurons systematically reduces the frequency-resolved amplification index across all frequencies (Fig 3A), confirming the steady-state analysis (cf. Fig 2B). Note that to control for the overall reduction in activity when recurrent inhibition is increased, we adjusted the time-independent external inputs such that the mean firing rates are kept constant in spite of changes in recurrent strength. In contrast to recurrent inhibition, spike-frequency adaptation introduces a prominent frequency selectivity: For low-frequency oscillations, the frequency-resolved amplification index decreases with increasing adaptation strength. For high-frequency oscillations, it increases (Fig 3B and 3C). Furthermore, the circuit exhibits a preferred frequency (resonance frequency), for which it yields a maximal response. This resonance frequency arises from an interplay of the rate and adaptation time constants. For low-frequency oscillations, adaptation is fast enough to track the input changes and hence able to suppress the frequency-resolved amplification index. With increasing stimulation frequency, this suppression weakens because adaptation is too slow. As a consequence, the oscillation amplitude increases with stimulation frequency. For high-frequency oscillations that are faster than the time constant of the firing rate, the frequency-resolved amplification index declines, because the neuron cannot react sufficiently quickly. Neuronal adaptation hence introduces a frequency-selective amplification that preferentially transmits specific neuronal rhythms within the broad spectrum of oscillations in the brain [43].

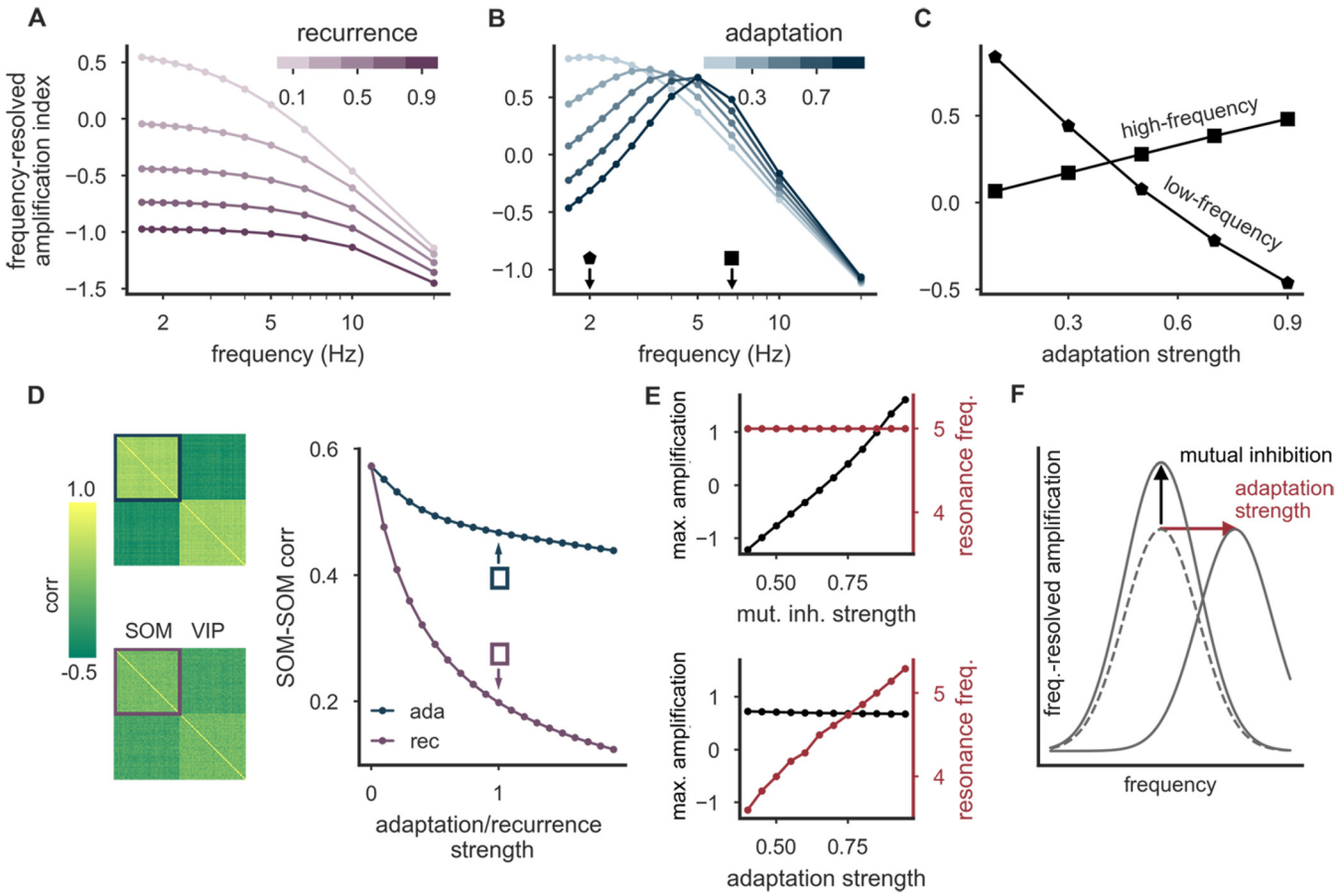

Fig 3. Spike-frequency adaptation enables frequency-selective amplification and preserves co-activity. (A) Frequency response analysis of the interneuron network with recurrent connections among both SOM and VIP neurons. Increasing recurrence reduces the frequency-resolved amplification index across all stimulation frequencies. **(B)** Same as in (A), but with spike-frequency adaptation instead of recurrence. The circuit yields a maximal response at a resonance frequency. With increasing adaptation strength, this resonance frequency increases. **(C)** The frequency-resolved amplification index decreases with increasing adaptation strength for low-frequency oscillations, but increases for high-frequency oscillations (frequency-selective amplification, cf. markers in (B)). **(D)** Neurons show stronger correlations (positive or negative) with spike-frequency adaptation (left, upper panel) than with recurrent inhibition among SOM and VIP neurons (left, lower panel). Mean SOM-SOM neuron correlation is more sensitive to increasing recurrence strength than to adaptation strength (right). **(E)** While strengthening mutual inhibition leads to an increase of the maximal frequency-resolved measure of amplification, it does not change the resonance frequency (top, adaptation strength $b = 0.8$). In contrast, increasing the adaptation strength allows to adjust the resonance frequency, with a weak impact on the maximum of the frequency-resolved amplification index (bottom, recurrence strength $\hat{w}_r = 0.8$). **(F)** Schematic representation of both separate "knobs" (mutual inhibition and adaptation) and their independent control of the amount and frequency-selectivity of the amplification. Parameter (A-E): Mutual inhibition strength $\hat{w} = 0.8$.

https://doi.org/10.1371/journal.pcbi.1006999.g003

Spike-frequency adaptation and recurrent inhibition also have distinguishable consequences for the correlation structure of the interneuron network. Karnani et al. (2016) [39] demonstrated that both SOM and VIP neurons are cooperatively active as populations rather than individually. We studied this co-activity by stimulating both interneuron populations with shared and individual noise on top of a constant background input. The shared noise between members of the same interneuron class introduced strong correlations between both VIP/VIP and SOM/SOM neurons as described by Karnani et al. [39]. We then studied how recurrent inhibition and adaptation differentially affect the co-activity of the populations, quantified by the averaged pairwise correlation coefficient. We found that recurrent inhibition strongly decreases the correlation between members of the same interneuron class [44]

(Fig 3D), while adaptation introduces only a marginal reduction, and thereby preserves the high correlations seen by Karnani et al. [39].

As for any amplifier, it would be useful to allow a dynamic adjustment of the amplification in the circuit. Very strong amplification would lead to small ranges of effective modulatory signals and a rapid saturation of the system, and hence to potential distortions in the translation of the modulatory signal into somatic and dendritic inhibition. Similarly, it could be beneficial to allow an adjustable frequency-based selection of the modulatory input. A neuronal mechanism that is suitable to tune these two properties could be a neuromodulatory control of circuit parameters [18, 35–38, 45]. In simulations, we found that a strengthening of mutual inhibition increases the overall amplification, while leaving the resonance frequency largely unaltered (Fig 3E, top). At the same time, changes of the adaptation strength allow to tune the resonance frequency, while leaving the maximum of the frequency-resolved measure of amplification largely unchanged (Fig 3E, bottom). In summary, the circuit seems to display separate "knobs", which offer an independent control of the amount and frequency-selectivity of the amplification through separate neuromodulatory channels (Fig 3F).

These results demonstrate that spike-frequency adaptation, though similar in its steady-state properties to recurrent inhibition within SOM and VIP populations, enables a frequency-selective amplification with well-separated target parameters for neuromodulatory control. While a neuromodulation of synaptic and cellular properties has been studied both for pyramidal cells [45, 46] and interneurons [18, 35–38, 47], it is not clear how strong the various forms of modulation are in vivo and how they interact on the circuit level. It therefore remains to be seen whether interneurons support a sufficient degree of neuromodulation of spike-frequency adaptation and mutual inhibition to dynamically tune the frequency selectivity of the circuit.

The computational repertoire of the SOM-VIP motif

Our simulations indicate that the SOM-VIP subnetwork supports different computational functions, ranging from signal amplification and frequency selection to switching behavior for strong mutual inhibition between the populations. To understand how these computational states are determined by the parameters of the system, we ran extensive simulations of the SOM-VIP motif alone, accompanied by mathematical analyses of a linearized network without rate rectification.

We first investigated a network of VIP and SOM neurons that is consistent with experimentally observed characteristics, i.e., with adaptation and inhibitory connections exclusively between neurons of different type. Simulations reveal four operating modes for such a network (Fig 4A). For weak mutual inhibition, the two interneuron populations can be active at the same time, and modulatory VIP signals are attenuated (Fig 4A, region (a)). As the inhibition between the two populations increases, the amplification index increases and leads the circuit into an amplification domain (Fig 4A, region (b)). Beyond a critical strength of mutual inhibition, the network then transitions into a switch-like winner-take-all domain (Fig 4A, regions (c) & (d)), in which one of the two populations silences the other. Notably, this state comes in two variants: For weak adaptation, the winning population silences the other permanently, or until an external event switches the network to a different winner (Fig 4A, region (c)). We will show later that this allows transient VIP inputs to persistently switch the operating mode in the full microcircuit. For strong adaptation, the network shows oscillations (Fig 4A, region (d)), because adaptation gradually decreases the firing rate of the winning interneuron population. This releases the other population from inhibition until it can no longer be silenced and becomes the new winner and in turn starts to adapt. A mathematical analysis of the linearized

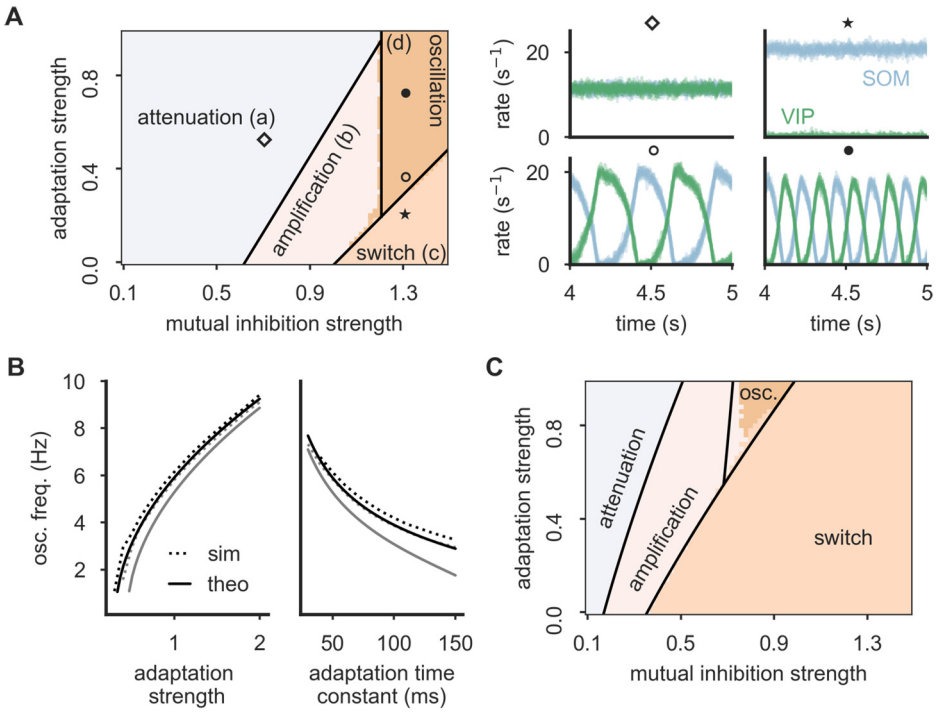

Fig 4. Dynamical states of the SOM-VIP motif. (A) Left: Bifurcation diagram reveals distinct operation modes: all interneurons are active (divided into amplification (a) and attenuation regime (b)), a winner-take-all (WTA) regime implementing a switch (c) and an oscillation regime (d). Regime boundaries (black lines) are obtained from a mathematical analysis (see S1 Appendix). Right: Example firing rate traces for all SOM (blue) and VIP (green) neurons for four network settings taken from the bifurcation diagram (cf. markers). Adaptation time constant $\tau_a = 50$ ms. **(B)** The oscillation frequency in the oscillation regime depends on the adaptation strength (left), the adaptation time constant (right) and the total mutual inhibition strength (black: $\hat{w} = 1.3$, gray: $\hat{w} = 1.4$). Left: $\tau_a = 50$ ms, right: $b = 1$. The frequencies cover a broad range from Delta to Alpha oscillations. **(C)** When short-term facilitation (STF) is present, the WTA (switch) regime is enlarged and the oscillation mode requires stronger adaptation. Initial synaptic efficacy $U_s = 0.1$, facilitation time constant $\tau_f = 100$ ms.

https://doi.org/10.1371/journal.pcbi.1006999.g004

network predicts the parameter ranges of the four computational states almost perfectly (see black lines in Fig 4A, and Methods for more details). The observed oscillations comprise a wide spectrum of frequencies that depend non-linearly on the strength and time constant of adaptation and on the strength of mutual inhibition (Fig 4B, see also S3 and S4 Figs for networks with asymmetric adaptation parameters for SOM and VIP neurons). Deviations between the frequencies observed in simulations and those predicted by the mathematical theory are caused by the omission of the rate rectification in the theory. The four computational states of the network are also observed when short-term plasticity is introduced into the network, although the transition boundaries change such that the switch-like state is reached for weaker mutual inhibition and the oscillation regime requires stronger adaptation (Fig 4C).

Two inhibitory populations that mutually inhibit each other may well be a common network motif in cortical circuits, and the absence of recurrent inhibitory connections within the two populations—as observed in the SOM-VIP motif—may not always hold. We therefore also performed an analysis of the computational states of a network with recurrent inhibition. Simulations reveal five operating modes for such networks (see S5 Fig). When mutual inhibition and recurrent inhibition is weak, we again found that both interneuron populations can be active at the same time. Depending on the strength of the mutual inhibition, we again observed attenuation and amplification, respectively. For sufficiently strong mutual inhibition

between SOM and VIP cells, the amplification regime transitions into the switch-like state where only one population is active. In contrast to adapting neurons, the network did not show an oscillatory state. Instead, very strong recurrent inhibition introduces strong competition between the neurons within the interneuron populations, leading to pathological states where either one single cell per cell type is active (if mutual inhibition is weak) or only one single neuron at all is active (if mutual inhibition is strong). Again, these dynamical states and their transitions are predicted almost perfectly by a mathematical eigenvalue analysis (see black lines in S5 Fig, and Methods for derivation). The mathematical analysis also unveils that for sufficiently large populations, the pathological states require very strong synapses (ultimately, a single cell must silence all others) and are hence unlikely to be observed in the nervous system.

In summary, the SOM-VIP network motif allows different computational states, covering attenuation, amplification, switching and—for adapting neurons— oscillations in a frequency range of Delta (1-4 Hz), Theta (4-8 Hz) or Alpha (8-12 Hz) oscillations.

Switch between distinct processing modes in local microcircuits

To investigate the computational consequences of the SOM-VIP circuit, we returned to the full microcircuit comprising PCs and inhibitory PV, SOM and VIP cells (S6 Fig). We first verified that all results observed in the simplified interneuron networks still hold for the larger circuit. Again, stronger mutual inhibition and the presence of STF increase, while negative feedback mechanisms like recurrent inhibition or adaptation decrease the system's sensitivity to the modulatory input (S6 Fig). Furthermore, adaptation leads to a frequency-selective amplification for which the processing of rapidly changing input signals benefits from powerful spike-frequency adaptation in SOM and VIP neurons (S6 Fig). Finally, the experimentally observed elevated correlation between members of the same interneuron class is also preserved for adaptation and decreases strongly for recurrent inhibition (S6 Fig). In summary, the results obtained in the simplified interneuron network also hold in the full circuit.

What is the computational impact of a somato-dendritic redistribution of inhibition on PCs? It is well established that on their apical dendrites, many pyramidal cells receive top-down input from higher cortical areas [22, 23] and matrix thalamic nuclei [24]. On their basal dendrites and the perisomatic domain, they receive bottom-up input from lower cortical areas and core thalamic nuclei [25]. Although inputs at the electrically distant apical dendrites have a small impact on initiating spikes at the axon initial segment [48, 49], they can initiate long-lasting calcium spikes when they coincide with back-propagating action potentials from the soma [50–52], leading to a significant gain increase of L5 pyramidal cells [53]. How the two streams of information are integrated is not fully resolved [54]. In particular, it is conceivable that top-down inputs are only used when they provide useful and reliable information, and are ignored otherwise. Given that calcium spikes in apical dendrites are very sensitive to inhibition [55], dendrite-targeting interneurons are well suited to control the integration of top-down inputs, and, consequently, the switch between distinct modes of operation. We therefore simulated the full microcircuit with top-down and bottom-up inputs, in a "switch" configuration of strong mutual inhibition between VIP and SOM, and without spike-frequency adaptation. For illustration, we chose as inputs two sinusoidal oscillations with different frequencies (Fig 5A & 5C), and determined how strongly these two input streams are represented in the firing rate of PCs (Fig 5A & 5B). When the network is in the "switch" regime, we found that small changes in VIP input are sufficient to switch the network between two computational states in which top-down inputs are either transmitted or cancelled entirely (Fig 5B). Interestingly, transitions between those two computational states can also be triggered by transient modulatory pulses.

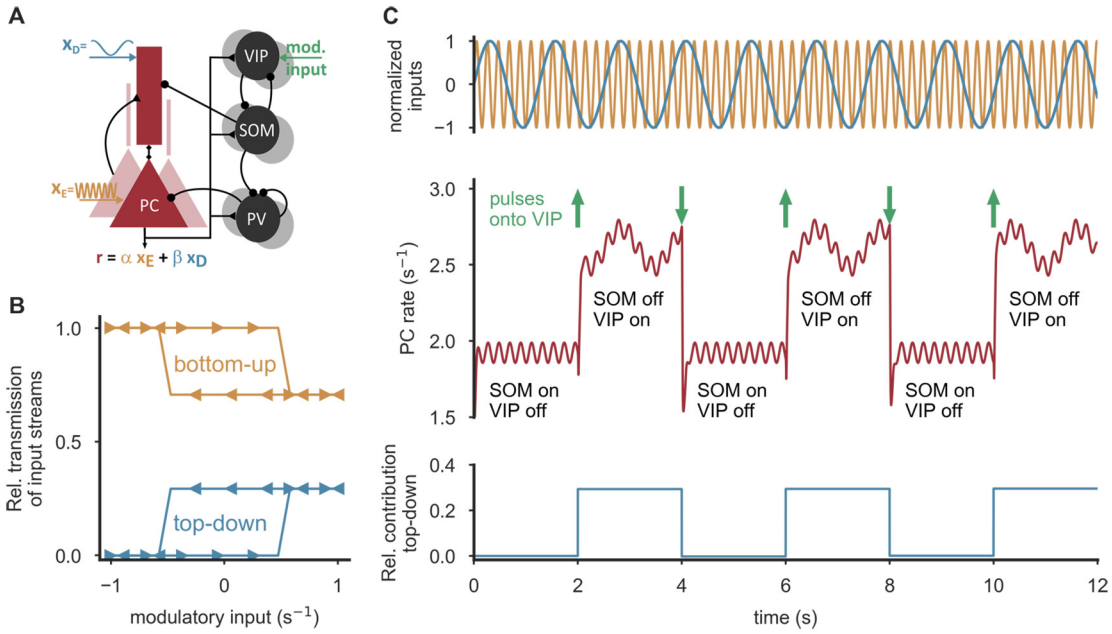

Fig 5. Integration or cancelation of top-down signals by modulatory VIP input. (A) PCs of the full microcircuit are stimulated at the soma and the apical dendrites with two oscillations with different frequencies, emulating bottom-up (orange, x_E) and top-down (blue, x_D) input, respectively. PC rate reflects the two inputs x_E and x_D with different coefficients α and β, depending on the modulatory input. **(B)** In an amplification regime ($\hat{w} = 1.1$), weak, permanent modulatory VIP input is sufficient to switch between two operation modes, in which top-down input is either integrated ($\beta > 0$) or cancelled ($\beta = 0$). In the WTA regime, the network exhibits hysteresis, that is, the level of modulatory input needed to cause a switch depends on the network state. For a range of inputs, the circuit is bistable. **(C)** In the bistable regime ($\hat{w} = 1.2$), persisting transitions between the states can be triggered by strong, short pulses delivered to VIP neurons (10 ms duration, amplitude 8.4/s, timing denoted by green arrows). Parameters (A-C): Weight between SOM neurons and dendrites $\hat{w}_{DS} = 2.8$, External stimulation $x_E = 25/s + 0.5 \sin(5\,t)/s$, $x_D = 7/s + 0.1 \sin(30\,t)/s$, $x_{PV} = 12/s$, $x_{SOM} = x_{VIP} = 3.5/s$.

https://doi.org/10.1371/journal.pcbi.1006999.g005

The evoked change of the processing mode persists even after the end of the pulse (Fig 5C), reflecting a bistability of the system. As a consequence, the current processing mode of the network depends on the recent history of the input to the SOM-VIP motif (S7 Fig).

In summary, we demonstrate that the integration of top-down feedback from higher cortical areas can be induced or prevented by persistent, weak input or short, strong input pulses onto VIP cells. As the network exhibits hysteresis, the switching depends on the collective state of SOM and VIP neurons.

Amplification of small mismatch signals

The SOM-VIP circuit can be interpreted as an amplifier for small differences between two inputs that impinge onto SOM and VIP neurons. We therefore simulated a network with two modulatory signals targeting SOM and VIP neurons. By systematically varying these inputs in an amplification regime, we verified that the somato-dendritic distribution of inhibition is determined by the mismatch between the two inputs (Fig 6A).

This observation is interesting in the context of a recent study of Attinger et al. (2017) [56]. The authors suggested a conceptual model for layer 2/3 of mouse V1, in which SOM neurons receive visual inputs, while VIP neurons and the apical dendrites of the PCs receive an internal (motor-related) prediction of the *expected* visual input. When properly tuned, the excitatory top-down input to the PC dendrites is then cancelled by SOM inhibition, as long as the internal prediction matches the sensory data. Deviations between sensory inputs and internal

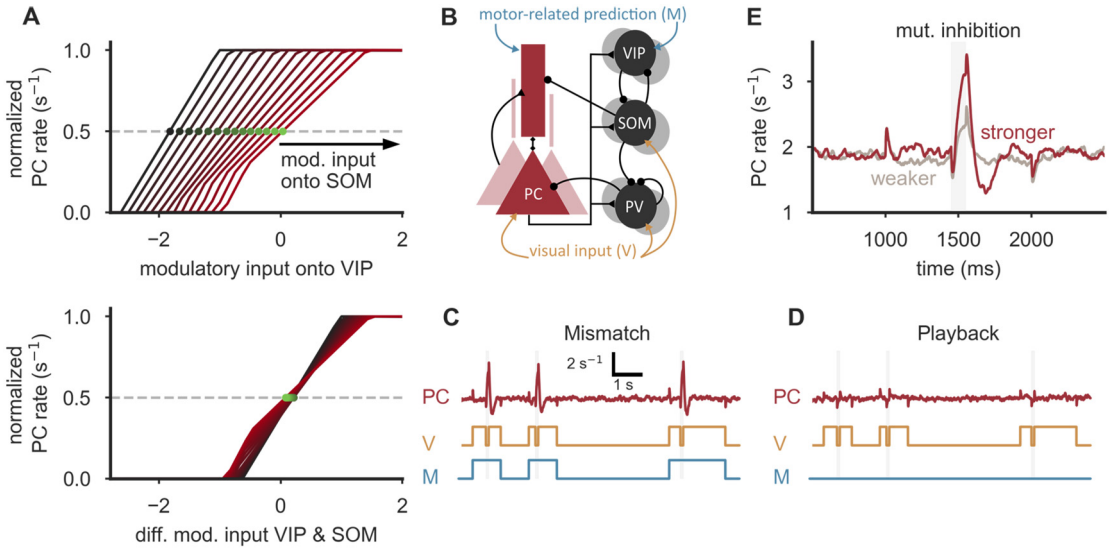

Fig 6. Mismatch detection by SOM/VIP-dependent amplification. (A) Additional modulatory input onto SOM neurons shifts the transition point (green) of the PC rate as a function of modulatory VIP input (top). When plotted as a function of the difference of SOM and VIP input, the transition points align, indicating that the circuit amplifies differences between two input streams (bottom). Additional input onto SOM neurons ranges from −2/s to 0/s. **(B)** Model for the integration of visual inputs and motor-related predictions [56]. SOM neurons, PV neurons and the somatic compartment of PCs receive external visual input, VIP neurons and the apical dendrites of PCs receive an internal (motor-related) prediction of the expected visual input. The connection strengths from PV neurons to the somatic compartment of PCs and the SOM→PV connection were chosen to ensure a response only when the visual input is switched off and the (motor-related) prediction is switched on (see S1 Appendix for details). **(C)** PCs respond with an increase in firing rate when visual input is off and the motor-related input is on (mismatch), but show a negligible increase in activity above baseline when both input streams are on. **(D)** Also, only negligible responses above baseline are evoked when motor-related input is permanently off (playback session). $\hat{w}_{SV} = 0.9$, $\hat{w}_{VS} = 1.1$. **(E)** The mismatch-induced increase in firing rate is more pronounced in an amplification regime ($\hat{w}_{SV} = 0.9$, $\hat{w}_{VS} = 1.1$, dark red) in comparison to an attenuation regime ($\hat{w}_{SV} = 0.1$, $\hat{w}_{VS} = 0.3$, gray). Parameters (B-E): Motor-related and visual input on corresponds to an additional input of 10.5/s and noise drawn from a Gaussian distribution with zero mean and SD = 3.5/s. Background stimulation $x_E = 28$/s, $x_D = 0$/s. Time constant of PCs increased by factor 6 to reduce onset responses.

https://doi.org/10.1371/journal.pcbi.1006999.g006

predictions, however, change the level of dendritic inhibition and thereby generate mismatch responses, as observed in a subset of PCs in V1 [56, 57] and in other systems [58, 59].

To test this hypothesis *in silico*, we stimulated our full circuit model with visual inputs—impinging onto PV and SOM neurons and the somata of PCs—and motor feedback—impinging onto VIP neurons and the apical compartment of PCs (Fig 6B). Similar to the findings of Keller et al. (2012) [56], we found network configurations in which we observed selective responses in PCs when motor feedback was present in the absence of visual stimulation (Fig 6C), but not when visual stimuli were presented in the absence of motor feedback (Fig 6D). These responses were reduced when the circuit was brought into an attenuation configuration by weakening mutual inhibition between VIP and SOM neurons (Fig 6E).

We therefore suggest that the amplification brought about by the competition between SOM and VIP neurons could serve to amplify small deviations between different input streams, such as sensory signals and internal predictions. Because such deviations are powerful learning signals for the internal prediction system [60], an amplification may be beneficial for learning highly accurate predictions.

Discussion

We have shown that the broadly observed microcircuit comprising excitatory PC and inhibitory PV, SOM and VIP neurons can act as an amplifier that translates weak input onto VIP

cells into large changes in the somato-dendritic distribution of inhibition onto PCs. A cornerstone of this amplification is mutual inhibition between SOM and VIP neurons that—if sufficiently strong—allows switch-like spatial shifts of somato-dendritic inhibition. Connectivity properties like short-term facilitation of those mutual connections and the absence of recurrent connections among both SOM and VIP neurons support the amplification. Spike-frequency adaptation as observed for SOM and VIP cells gives rise to a frequency-selective amplification, as a consequence of the slow time scales of adaptation. Furthermore, adaptation in conjunction with sufficiently strong mutual inhibition results in an oscillation regime, in which SOM and VIP neurons alternately win the competition, thus generating rhythmic shifting of somato-dendritic inhibition. These oscillations are inherited by PCs that fluctuate between two different computational states with frequencies ranging from approximately 1 to 10 Hz. Functionally, such oscillations could reflect a rhythmic switching between a state in which sensory data is acquired and a state in which it is calibrated against internal predictions.

A strong amplification is inextricably linked with a small dynamic range, in which modulatory signals influence the output. This trade-off is an intrinsic property of any amplifier and cannot be circumvented. An efficient transmission of modulatory signals would require to align the statistics of the modulatory input and the dynamic range of the amplifier. We hypothesize that this could be achieved by plasticity within the SOM-VIP motif. Which plasticity rules could achieve such an alignment is beyond the scope of the present work. Whether the SOM-VIP motif would act as an attenuator, amplifier, switch or oscillator depends on details of the circuit and should be task- and area-specific.

The microcircuit we studied has been observed in several cortical areas, including mouse primary somatosensory (S1), visual (V1) and vibrissal motor (vM1) cortex, and both in layer 2/3 and 5 [12, 13, 15, 26–32]. We did not strive to resolve subtle differences between these areas, but rather covered broad parameter ranges to explore the computational repertoire of the circuit (see, e.g., [61] for area-to-area variations). We suggest that the observed architecture of the microcircuit is consistent with the function of an amplifier for modulatory signals, but an amplification could of course also be achieved by different mechanisms, such as non-linear input-output (transfer) function with steep (switch-like) slope for SOM or VIP neurons or very strong synapses for modulatory inputs. It can be assumed that the brain employs a number of different co-existing mechanisms to achieve a high amplification index when needed.

The absence of recurrent connections among both SOM and VIP neurons has been supported by many studies, both in vitro and in vivo [13, 39]. It has been argued, however, that SOM neurons should be subdivided into 'Martinotti' and 'non-Martinotti' cells to account for differences in their morphology and biophysical properties [15]. While recurrence seems to be weak or absent within both sub-populations, connections between these subgroups have been reported. However, most of the SOM neurons belong to the class of Martinotti cells that avoid connections to each other. The majority of the 'non-Martinotti' cells recorded by Jiang et al. [15] were classified as basket cells which target the somatic compartment of the PCs, suggesting that within our model, they would fall into the category of soma-targeting cells rather than into the class of dendrite-targeting cells. A detailed analysis of the consequences of splitting up these two cell classes is beyond the scope of the present study.

Following the model of Murayama et al. (2009) [34], recurrent excitation among PCs targets the dendritic compartment. However, the results presented here remain qualitatively unaltered if recurrent excitation targets the somatic compartment instead, because we considered a homogeneous population of PCs, in which excitatory recurrent connections served no

specific purpose. In other contexts, in which recurrent excitation plays a particular role, the question of whether an inhibitory control of the top-down input also affects recurrent excitatory processing can have profound consequences.

The model contained a unidirectional connection from SOM neurons onto PV neurons. This assumption is based on the common observation that this connection is strong and frequent, while the backprojection is rather weak or absent in layer 2/3 and 5 [13, 16]. An exception is the study of Walker et al. (2016) [62], who reported strong and frequent connections from PV to Martinotti cells in layer 2/3 of mouse S1. We expect that such a mutual inhibition between PV and SOM neurons would not violate our hypothesis, but rather introduce another amplification mechanism with a similar structure. However, PV→SOM connections may also introduce complex interactions between inputs to PV and VIP neurons that are not captured in our model. It remains for future work to explore the computational and functional consequences of such serially connected amplifiers.

In our model, VIP neurons are connected exclusively to SOM neurons. We neglected potential VIP input to PCs and other interneuron classes. This assumption is supported by a wealth of experimental studies that reported no or weak connections from VIP to PC and PV neurons [13, 15, 17]. However, in a study of Garcia-Junco-Clemente et al. (2017) [63] strong and direct connections between VIP neurons and PCs were found during arousal in layer 2/3 of the mouse frontal association area. The strength of this inhibition was highly variable between cells, covering a wide range of almost two orders of magnitude. Also, this connection was reported to be weaker in the occipital cortex in the same study [63]. Notwithstanding the presence of this connection in different systems, it is tempting to speculate on its computational function, because it may enable to run different operating modes in parallel. Karnani et al. (2016) [39] have demonstrated that SOM and VIP neurons receive local excitation from distinct (non-overlapping) PC groups rather than non-selectively from all nearby excitatory neurons. If the respective interneuron types also selectively project back, and if the VIP projection would also impinge onto apical dendrites, one group of PCs may operate in a feedback-modulated state, whereas another group runs in a feedforward-driven mode at the same time (see Fig 7).

In our model, we assume that the activation of VIP neurons leads to a disinhibition of PCs through the suppression of SOM cells. This net disinhibitory effect has been observed in S1 [29], V1 [13, 17–19] and the auditory cortex [17]. However, data from a recent study [64] challenges the perspective of a sole disinhibitory impact by showing an increase of SOM activity in the presence of visual stimuli during locomotion. In a theoretical study by del

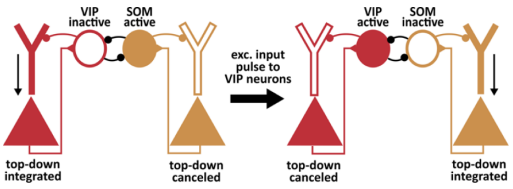

Fig 7. Diverse processing modes at the network level. Garcia-Junco-Clemente et al. (2017) [63] suggested that VIP neurons also target the apical dendrites of PCs. Moreover, Karnani et al. (2016) [39] suggested that SOM and VIP neuron populations receive excitatory input from distinct (non-overlapping) PC populations. If SOM and VIP interneurons preferably inhibited those PCs from which they get their input, it is conceivable that the distinct PC populations operate in a feedback-modulated state and a feedforward-driven mode, respectively. The switch between these states could then be triggered by VIP neuron input or the difference between modulatory input onto SOM and VIP cells.

https://doi.org/10.1371/journal.pcbi.1006999.g007

Molino et al. (2017) [65], this response reversal has been explained by the interaction of multiple neuron types, and different baseline activity levels due to non-linear input-output functions. This non-linearity is not present in our model, and hence, we cannot model response reversal effects.

The modulatory VIP neuron input in our microcircuit represents an abstract control signal. We deliberately did not specify the origin of this signal throughout most of this study, because inputs to VIP cells are very diverse. Besides local excitation from PCs in the same and deep layers, the greatest source of excitatory input of VIP cells is feedback from higher cortical areas and thalamus [3, 66, 67]. Moreover, VIP neurons are also strongly excited by acetylcholine and serotonin [66], and Pi et al. (2013) [17] have shown that VIP neurons in the auditory and prefrontal areas are recruited by reinforcement signals during an auditory discrimination task. Furthermore, in barrel cortex, VIP cells increase their activity during whisking as they receive substantial input from vM1 pyramidal neurons [29]. Finally, it has been shown that locomotion activates VIP cells in V1 (independent of visual stimulation) and their firing rate is correlated with running speed [18]. In summary, the assumption of a modulatory signal targeting VIP cells is supported by experimental data, but its origin or functional meaning may well vary between areas or over time.

Modulatory inputs may not comprise inputs to VIP neurons alone. The ability to amplify weak signals arriving in the SOM-VIP motif may be of particular importance in the context of detecting mismatches between two sources of information [56, 57]. This could allow not only to amplify, but also to compute error signals that drive the refinement of internal models or the computational function of hierarchical "deep" networks [68–71].

The ability to switch between distinct operating modes increases the computational repertoire of principal cells. When SOM neurons are inactive, top-down inputs onto apical dendrites elevate the output of pyramidal cells, for instance by bursts generated by dendritic calcium spikes [25]. On the other hand, when SOM neurons are highly active, the transmission of dendritic signals can be effectively cancelled. Feedback "top-down" projections have been associated with a variety of cognitive parameters, including attention and visual awareness [68, 72, 73], context [68, 72, 74], internal predictions of the outside world [25, 72, 75] and error or reinforcement signals for learning [68–71]. Hence, the integration or cancellation of top-down inputs from higher to lower cortical areas is likely to play a crucial role in information processing, cognition and perception [25, 72, 73]. The SOM-VIP microcircuit could enable an efficient control over these processes by cortical and thalamic inputs to VIP neurons [18, 19, 29, 67]. We did not strive to resolve branch-specific (dis-)inhibition effects but rather considered a blanket of inhibition that suppresses the dendritic tree as a whole. Pathway-specific gating has been investigated in a network comprising several interneuron types [76]. The authors suggest that signals reflecting distinct, sensory modalities arriving at different branches of the dendritic tree can be selectively forwarded to the soma by releasing the target branch from SOM-mediated inhibition. More generally, our model does not account for intricate non-linear interactions in spatially extended dendrites that are observed in detailed compartmental models [77–79]. Therefore, it is conceivable that taking into account spatially extended dendrites with a rich arborization could further enhance the computational repertoire of the system.

Despite the accumulating data on the broad variety of interneurons [3], their computational function is still poorly understood. The present study provides a hypothesis for one candidate function: An effective redistribution of inhibition along the somato-dendritic axis by an amplification of small control signals within the SOM-VIP motif. Functionally, we have shown that this can control whether top-down input is integrated or cancelled. This computational role may well be only one in a broad repertoire of functions performed in parallel. Computational

models may offer a useful resource to understanding this functional repertoire [65, 76, 80–83], given that they offer a degree of control over the circuit that is hard to achieve in experimental setups.

Methods

Neural network model

We simulated a rate-based network of excitatory pyramidal cells ($N_{PC} = 70$) and inhibitory PV, SOM and VIP cells ($N_{PV} = N_{SOM} = N_{VIP} = 10$). All neurons are randomly connected with connection probabilities (see Table 1) consistent with the experimental literature [12, 13, 15]. If not stated otherwise, all cells of the same neuron type have the same number of incoming and outgoing connections, respectively. This assumption is made merely for purposes of mathematical tractability and does not qualitatively alter the results.

The excitatory pyramidal cells are simulated by a two-compartment rate model taken from [34]. The steady-state firing rate $r_{E,i}$ of the somatic compartment of neuron i obeys

$$\tau_E \frac{dr_{E,i}}{dt} = -r_{E,i} + [I_i - \Theta]_+, \tag{1}$$

where $[x]_+ = max(0, x)$ is a rectifying nonlinearity and τ_E denotes a rate time constant ($\tau_E = 10$ ms, unless stated otherwise). Θ denotes the rheobase of the neuron and I_i is the total somatic input generated by somatic and dendritic synaptic events and potential dendritic calcium spikes,

$$I_i = \lambda_D[I^{syn}_{D,i} + c_i]_+ + (1 - \lambda_E)I^{syn}_{E,i}. \tag{2}$$

$I^{syn}_{D,i}$ and $I^{syn}_{E,i}$ are the total synaptic inputs into dendrites and soma, respectively, and c_i denotes the dendritic calcium event. λ_D and λ_E are the fraction of "currents" leaking away from dendrites and soma, respectively. The synaptic input to the soma $I^{syn}_{E,i}$ is given by the sum of external bottom-up inputs x_E and PV neuron-induced (P) inhibition,

$$I^{syn}_{E,i} = x_E - \sum_{j=1}^{N_{PV}} w_{EP,ij}\, r_{P,j}. \tag{3}$$

$I^{syn}_{D,i}$ is the sum of top-down inputs x_D, the recurrent, excitatory connections from other PCs and SOM neuron-induced (S) inhibition:

$$I^{syn}_{D,i} = x_D - \sum_{j=1}^{N_{SOM}} w_{DS,ij}\; r_{S,j} + \sum_{j=1}^{N_{PC}} w_{DE,ij}\; r_{E,j}. \tag{4}$$

The weight matrices w_{EP}, w_{DS} and w_{DE} denote the strength of connection between PV neurons and the soma of PCs (w_{EP}), SOM neurons and the dendrites of PCs (w_{DS}) and the recurrence strength between PCs (w_{DE}), respectively (see Table 2). Note that all existing connections between neurons of type X and Y have the same strength, $w_{XY,ij} = w_{XY}$, $X, Y \in \{E, D, P, S, V\}$. All weights are scaled in proportion to the number of existing connections (i.e., the product of the number of presynaptic neurons and the connection probability), so that the results are independent of population sizes. The input generated by a calcium spike is given by

$$c_i = c \cdot H(I^0_{D,i} - \Theta_c), \tag{5}$$

where c scales the amount of current, H is the Heaviside step function, Θ_c represents a threshold that describes the minimal input needed to produce a Ca^{2+}-spike and $I^0_{D,i}$ denotes the total, synaptically generated input in the dendrites,

$$I^0_{D,i} = \lambda_E I^{syn}_{E,i} + (1 - \lambda_D) I^{syn}_{D,i}. \tag{6}$$

Unless stated otherwise, parameters were taken from [34] (see Table 2). Note that we incorporated the gain factor present in Murayama et al. (2009) [34] into the parameters to achieve unit consistency for all neuron types.

The firing rate dynamics of each interneuron is modeled by a rectified, linear differential equation [33]:

$$\begin{aligned} &\tau_i \ \dot{r}_i = -r_i + \sum_j w_{ij} \, u_{ij} \, r_j - a_i + x_i, \\ &(\text{if } \ r_i < 0, \ \ \text{then } \ r_i \to 0) \end{aligned} \tag{7}$$

where a_i represents an adaptation variable, w_{ij} denotes the relevant synaptic weight onto the neuron, u_{ij} describes a synaptic facilitation variable and x_i denotes external inputs. The rate time constant τ_i was chosen to resemble the $GABA_A$ time constant of approximately 10 ms for all interneuron types included. The weight matrix W (see Table 3) was chosen such that the relative connection strengths are consistent with experimental findings [12, 13, 15, 17, 29]. When we simulated mismatch neurons (see Fig 6, main text), we set the total SOM→PV connection strength to $\hat{w}_{PS} = 0.2$, the total PV→PV weight to $\hat{w}_{PS} = 1.0$, and tuned the total synaptic strength from PV neurons to the somatic compartment of PCs in order to ensure a response only when the visual input is switched off and the (motor-related) prediction is switched on: $\hat{w}_{EP} = (1 + \hat{w}_{PP})/(1 - \hat{w}_{PS})$. Note that the total weight is given by the product of the number of existing connections between two neuron types and the strength for individual connections.

In contrast to PV neurons, both SOM and VIP cells show pronounced spike-frequency adaptation [3, 5, 6, 11, 16], which is described by an adaptation variable a_i,

$$\tau_a \ \dot{a}_i = -a_i + b \, r_i. \tag{8}$$

At constant neuronal activity r_i, the adaptation variable a_i exponentially approaches the steady-state value $b \, r_i$ with time constant τ_a. For simplicity, if not otherwise stated, the adaptation strength b and time constant τ_a are the same for both cell types ($b \in [0, 2]$, $\tau_a = 100$ ms). If adaptation is not present, we set the parameter b to zero.

Short-term facilitation is only modeled for SOM→VIP and VIP→SOM connections. The facilitation variable u_{ij} between neuron j and neuron i evolves according to the Tsodyks-Markram model [40, 41]:

$$\dot{u}_{ij} = \frac{U_s - u_{ij}}{\tau_f} + U_s(1 - u_{ij}) r_j. \tag{9}$$

The facilitation variable u_{ij} ranges from 0 to 1 and represents the release probability, which changes according to the availability of calcium in the axon terminals. In the absence of presynaptic activity, the facilitation variable u_{ij} relaxes exponentially with time constant τ_f to a steady state U_s, which represents the initial release probability. Presynaptic activity increases the facilitation variable u_{ij} by an amount proportional to U_s. If not stated otherwise, the initial release probability U_s and facilitation time constant τ_f are equal for SOM and VIP neurons ($U_s \in [0, 1]$, $\tau_f = 200$ ms). When STF is not present, $u_{ij} = 1$ (or, equivalently, $U_s = 1$). In

simulations where the strength of short-term facilitation is varied, we ensured comparability by scaling the weights w_{ij} by U_s, thereby keeping constant the initial synaptic response after a long period of inactivity.

External stimulation

To achieve physiologically reasonable activity levels, all neurons are stimulated with a time-independent background rate x_i. PCs receive constant bottom-up input x_E at the soma and top-down feedback x_D at their dendrites. Additionally, VIP (in the full network setting) or SOM neurons (in the reference network) receive an external stimulus x_{mod} that was varied systematically to investigate the amplification properties of the microcircuit. If not indicated differently, all cells of the same neuron type are presented with an identical stimulus.

In the interneuron network, for the sake of comparability across different parameter settings, we always adjust the background inputs x_i such that the spontaneous activity (that is, at $x_{mod} = 0$) is equal to $r_0 = 3/s$ for all interneurons. In the non-WTA regime this can be achieved by

$$x_i = (1 + b)\, r_{0,i} - \sum_j w_{ij}\, u_{ij}\, r_{0,j} \tag{10}$$

with $u_{ij} = 1$, if short-term facilitation is not present, or

$$u_{ij} = \frac{U_s(1 + \tau_f\, r_{0,j})}{1 + U_s\, \tau_f\, r_{0,j}} \tag{11}$$

otherwise. In the full microcircuit comprising PC, PV, SOM and VIP cells, the external stimulation is set to $x_{PV} = x_{SOM} = x_{VIP} = 3/s$ for the interneurons and $x_E = 17.5/s$ and $x_D = 21/s$ for the PCs, if not otherwise stated.

To characterize the dynamics of the system, we perform a frequency response analysis that measures the amplitude of the output signal as a function of the frequency $1/T$. In that case, the weak external stimulus x_{mod} is expressed by a sine wave

$$x_{mod} = \sin\left(\frac{2\pi t}{T}\right), \tag{12}$$

where $T \in [50, 600]$ *ms*. The frequency-resolved amplification index is then given by the logarithm of the ratio of the oscillation amplitudes in full and reference networks.

To investigate correlations, we stimulated SOM and VIP neurons with an input consisting of i) a constant component $\bar{x}$ (calculated as before, see Eq (10)), ii) individual noise and iii) noise that it shared among the neurons of the same type:

$$x_{mod,i} = \bar{x}(1 + 0.6\, \xi_{shared} + 0.4\, \xi_i)\,, \tag{13}$$

where the noise terms ξ_{shared} and ξ_i are drawn at each time t from Gaussian distributions with zero mean and unit variance. The shared component of the noise accounts for the strong correlations seen by Karnani et al. (2016) [39]. Furthermore, the number of cells per neuron type is increased in these simulations by a factor 5 to obtain reliable statistical estimates.

For the example firing rate traces (in Fig 4 and S3 & S4 Figs), we stimulated SOM and VIP neurons with an input consisting of i) a constant component of $25/s$ and ii) individual noise drawn at each time t from a Gaussian distribution with zero mean and SD of $5/s$.

Definition and mathematical derivation of the amplification index

To quantify the strength of amplification in our neural microcircuit, we introduce the amplification index,

$$A = \log_2\left(\frac{m_{\text{full}}}{m_{\text{ref}}}\right), \tag{14}$$

where m_{full} and m_{ref} denote the slope of the sigmoid function of the full and the reference network (see Fig 1D or 1F), respectively. These slopes represent the redistribution of somatic and dendritic inhibition upon a change in modulatory VIP input. Hence, the amplification index measures how much stronger the redistribution is when weak input passes through the SOM-VIP motif instead of directly through the SOM neurons.

The amplification index can be calculated analytically for the simplified linear network without PCs and short-term facilitation. To this end, we first derive the slope m_{full} from the mean-field population dynamics,

$$\tau\frac{dr_{\text{PV}}}{dt} = x_{\text{PV}} - (1+\hat{w}_{\text{PP}})\,r_{\text{PV}} - \hat{w}_{\text{PS}}\,r_{\text{SOM}}, \tag{15}$$

$$\tau\frac{dr_{\text{SOM}}}{dt} = x_{\text{SOM}} - (1+\hat{w}_{\text{SS}})\,r_{\text{SOM}} - \hat{w}_{\text{SV}}\,r_{\text{VIP}}, \tag{16}$$

$$\tau\frac{dr_{\text{VIP}}}{dt} = x_{\text{VIP}} + x_{\text{mod}} - (1+\hat{w}_{\text{VV}})\,r_{\text{VIP}} - \hat{w}_{\text{VS}}\,r_{\text{SOM}}, \tag{17}$$

where $\hat{w}_{mn}$ denotes the total weight from neuron type n onto m, and the rates r_n denote the mean-field population rate of neuron type n. For the sake of generality, we included the possibility of recurrent connections among both SOM and VIP neurons. Solving this set of equations for the steady-state population activity yields

$$r_{\text{PV}} = \frac{x_{\text{PV}} - \hat{w}_{\text{PS}}\,r_{\text{SOM}}}{1+\hat{w}_{\text{PP}}}, \tag{18}$$

$$r_{\text{SOM}} = \frac{x_{\text{SOM}}(1+\hat{w}_{\text{VV}}) - \hat{w}_{\text{SV}}(x_{\text{VIP}}+x_{\text{mod}})}{(1+\hat{w}_{\text{SS}})(1+\hat{w}_{\text{VV}}) - \hat{w}_{\text{SV}}\hat{w}_{\text{VS}}}. \tag{19}$$

The slope m_{full} is given by the derivative of $r_{\text{PV}} - r_{SOM}$ with respect to x_{mod},

$$m_{\text{full}} = \left(1+\frac{\hat{w}_{\text{PS}}}{1+\hat{w}_{\text{PP}}}\right)\frac{\hat{w}_{\text{SV}}}{(1+\hat{w}_{\text{SS}})(1+\hat{w}_{\text{VV}}) - \hat{w}_{\text{SV}}\hat{w}_{\text{VS}}}. \tag{20}$$

Similarly, the slope m_{ref} in the reference network can be derived from the mean field equations without VIP neurons and PCs,

$$\tau\frac{dr_{\text{PV}}}{dt} = x_{\text{PV}} - \hat{w}_{\text{PP}}\,r_{\text{PV}} - \hat{w}_{\text{PS}}\,r_{\text{SOM}}, \tag{21}$$

$$\tau\frac{dr_{\text{SOM}}}{dt} = x_{\text{SOM}} - x_{\text{mod}} - \hat{w}_{\text{SS}}\,r_{\text{SOM}}, \tag{22}$$

and is given by

$$m_{\mathrm{ref}} = \left(1 + \frac{\hat{w}_{\mathrm{PS}}}{1 + \hat{w}_{\mathrm{PP}}}\right) \frac{1}{1 + \hat{w}_{\mathrm{SS}}}. \tag{23}$$

Finally, the amplification index is given by the ratio of the slopes,

$$A = \log_2\left(\frac{m_{\mathrm{full}}}{m_{\mathrm{ref}}}\right) = \log_2\left(\frac{\hat{w}_{\mathrm{SV}}(1 + \hat{w}_{\mathrm{SS}})}{(1 + \hat{w}_{\mathrm{SS}})(1 + \hat{w}_{\mathrm{VV}}) - \hat{w}_{\mathrm{SV}}\hat{w}_{\mathrm{VS}}}\right). \tag{24}$$

In the absence of recurrent inhibition within SOM and VIP populations, this expression simplifies to

$$A = \log_2\left(\frac{\hat{w}_{\mathrm{SV}}}{1 - \hat{w}_{\mathrm{SV}}\hat{w}_{\mathrm{VS}}}\right). \tag{25}$$

Mathematical analysis of the computational repertoire of the SOM-VIP network

To analyze the computational repertoire of the SOM-VIP motif, we considered a network composed of SOM (hereafter only S) and VIP neurons (hereafter only V) that are mutually and fully connected. Again, the rectifying nonlinearity of the neurons is neglected.

Computational states with recurrent inhibition within SOM and VIP neurons. In the absence of adaptation, the dynamics of the system is fully characterized by the change in rates. Each population comprises n cells, so the dynamics of the full network are described by a $(2 \times n)$-dimensional system of linear differential equations,

$$\dot{\mathbf{r}} = W\mathbf{r} + \mathbf{s} \tag{26}$$

with $\mathbf{r}^{\mathrm{T}} = [r_{\mathrm{S}_1}, \ldots, r_{\mathrm{S}_n}, r_{\mathrm{V}_1}, \ldots, r_{\mathrm{V}_n}]$. $\mathbf{s}$ represents a vector of external stimuli and W is a block matrix that contains the connection weights.

By deriving the eigenvalue spectrum of the matrix W (see S1 Appendix for a detailed derivation), we can perform a bifurcation analysis. For the sake of simplicity, we suppose that the rate time constants, recurrence and mutual inhibition strengths are equal for both interneuron types: $\tau_{\mathrm{S}} = \tau_{\mathrm{V}} = \tau$, $w_{\mathrm{SS}} = w_{\mathrm{VV}} = w_{\mathrm{r}}$ and $w_{\mathrm{SV}} = w_{\mathrm{VS}} = w$. By analyzing the sign and nature (complex or real) of the eigenvalues, we can define five dynamical regimes:

(i) All interneurons can be active and operate in an attenuation regime,

(ii) All interneurons can be active and operate in an amplification regime,

(iii) Winner-take-all (WTA) between SOM and VIP neuron population (strong competition, either all SOM or all VIP cells are silenced, neurons within the winning population are all active),

(iv) WTA in each population separately (exactly one VIP and one SOM cell remain active),

(V) Total WTA (only one single neuron in the whole network is active).

The transition between the attenuation and the amplification regime ((i) and (ii)) is determined by the condition that the amplification index, Eq (24), is equal to one (for the symmetric case $\hat{w}_{\mathrm{VV}} = \hat{w}_{\mathrm{SS}} = \hat{w}_r$ and $\hat{w}_{\mathrm{SV}} = \hat{w}_{\mathrm{VS}} = \hat{w}$). The transition to WTA regimes ((iv) and (v)) within each neuron population emerges when the total recurrence strength $\hat{w}_{\mathrm{r}}$ is greater or

equal to the leak multiplied by the population size,

$$\hat{w}_{\mathrm{r}} \geq n - 1. \tag{27}$$

Moreover, the transition to a WTA regime between SOM and VIP neurons (regime (iii)) occurs when the total mutual inhibition strength $\hat{w}$ is larger than the sum of total recurrence $\hat{w}_{\mathrm{r}}$ and leak,

$$\hat{w}^2 > (1 + \hat{w}_{\mathrm{r}})^2, \tag{28}$$

where $\hat{w}_{\mathrm{r}} = (n-1)\, w_{\mathrm{r}}$ and $\hat{w} = n\, w$. Finally, the pathological regime (v) of a total WTA requires that Eq (27) is fulfilled and that $\hat{w} > n$, i.e., condition (28) at the transition boundary to WTA within the two populations.

Computational states with adaptation. In order to derive the qualitative changes in the bifurcation structure when adaptation (instead of recurrence) is present, we extended the rate-dynamics (see Eq (26)) with linear differential equations describing the evolution of an adaptation current (cf. Eq (8)). The $(4 \times n)$-dimensional state-vector $\mathbf{r}$ is now given by $\mathbf{r}^{\mathrm{T}} = [r_{\mathrm{S}_1}, a_{\mathrm{S}_1}, \ldots, r_{\mathrm{S}_n}, a_{\mathrm{S}_n}, r_{\mathrm{V}_1}, a_{\mathrm{V}_1}, \ldots, r_{\mathrm{V}_n}, a_{\mathrm{V}_n}]$. For the sake of simplicity and comparability, we suppose that the rate time constants, the mutual inhibition strength as well as the adaptation parameters are equal for SOM and VIP neurons: $\tau_{\mathrm{S}} = \tau_{\mathrm{V}} = \tau$, $w_{\mathrm{SV}} = w_{\mathrm{VS}} = w$, $b_{\mathrm{S}} = b_{\mathrm{V}} = b$ and $\tau_{\mathrm{a,S}} = \tau_{\mathrm{a,V}} = \tau_{\mathrm{a}}$. This symmetry simplifies the derivation of the eigenvalues considerably (see S1 Appendix).

The eigenvalue spectrum reveals that, in contrast to recurrence, adaptation does not lead to pathological states (see conditions (iv) and (v) in subsection above). Furthermore, depending on the sign and nature of the eigenvalues, we find four dynamical regimes:

(i) All interneurons can be active and operate in an attenuation regime (Fig 4A, region (a)),

(ii) All interneurons can be active and operate in an amplification regime (Fig 4A, region (b)),

(iii) Switch regime (Fig 4A, region (c)): WTA between SOM and VIP neuron population when total mutual inhibition strength is larger than the sum of the adaptation strength and the leak:

$$\hat{w} \geq b + 1. \tag{29}$$

(iv) Oscillation regime (Fig 4A, region (d)), in which SOM and VIP cells alternate between active and inactive states. It requires two conditions: First, adaptation must be stronger than the difference of total mutual inhibition and leak. Second, this total reciprocal inhibition must be larger than leak and ratio of rate and adaptation time constant:

$$\begin{aligned} b &> \hat{w} - 1, \\ \hat{w} &> 1 + \tau/\tau_{\mathrm{a}}. \end{aligned} \tag{30}$$

The derivation of the amplification index A for a network with adaptation is analogous to the derivation with recurrent inhibition, and merely requires to replace the total recurrence strength $\hat{w}_r$ by the strength b of adaptation. Hence, the transition between the attenuation and the amplification regime ((i) and (ii)) is determined by this minor modification of Eq (24).

In the oscillation regime, some of the eigenvalues of the dynamical system are complex. An approximation of the oscillation frequency can then be derived from their imaginary part:

$$f = \frac{1}{4\pi}\sqrt{\frac{4b}{\tau\tau_a} - \left(\frac{1}{\tau} - \frac{1}{\tau_a} - \frac{\hat{w}}{\tau}\right)^2}. \quad (31)$$

Simulation details and code availability

All simulations were performed in customized Python code written by LH. Differential equations were numerically integrated using a 2nd-order Runge-Kutta method with a maximum time step of 0.05 ms. Neurons were initialized with $r_i(0) = 0$ Hz, $a_i(0) = 0$ Hz (if adaptation was modeled) and $u_{ij}(0) = U_s$ (if STF was present) for all i. Source code will be made publicly available upon publication.

Supporting information

S1 Fig. Asymmetric mutual inhibition strengths for SOM and VIP neurons also enhances the amplification index. When one of the connections, VIP→SOM ($\hat{w}_{SV}$) or SOM→VIP ($\hat{w}_{VS}$), is kept constant, increasing the respective other weight leads to a strengthening of the amplification. Fixed weight was set to $\hat{w}_{VS/SV=1}$.
(PDF)

S2 Fig. Asymmetric recurrence strengths for SOM and VIP neurons also reduce the amplification index. When one of the recurrent connections, VIP→VIP ($\hat{w}_{VV}$) or SOM→SOM ($\hat{w}_{SS}$), is kept constant, increasing the respective other weight leads to a decrease of the amplification index. Fixed weight was set to $\hat{w}_{SS/VV=0.5}$. Mutual inhibition strength $\hat{w} = 0.8$.
(PDF)

S3 Fig. Oscillations also arise for asymmetric adaptation strengths in SOM and VIP neurons, with altered firing rate and oscillation frequency. Firing rate traces for SOM (blue) and VIP (green) neurons for a range of adaptation strengths ($b_{S/V} \in \{0.4, 0.6, 0.8, 1\}$). Off-diagonal plots correspond to asymmetric adaptation strengths. Mutual inhibition strength $\hat{w} = 1.3$, adaptation time constants $\tau_a = 50$ ms.
(PDF)

S4 Fig. Asymmetric adaptation time constants for SOM and VIP neurons lead to different duration of active and inactive periods. Firing rate traces for SOM (blue) and VIP (green) neurons for a range of adaptation time constants ($\tau_{a,S/V} \in \{50, 100, 200, 400\}$ ms). Larger adaptation time constants cause longer active states. Mutual inhibition strength $\hat{w} = 1.3$, Adaptation strength $b = 0.5$.
(PDF)

S5 Fig. Dynamical states of the SOM-VIP motif with recurrence. Left: Bifurcation diagram reveals distinct operation modes: all interneurons are active (divided into amplification and attenuation regime), winner-take-all (WTA) regime leading to a switch, and two pathological states (WTA in each population separately and total WTA). Regime boundaries (black lines) are obtained from a mathematical analysis (see S1 Appendix). Right: Example firing rate traces for all SOM (blue) and VIP (green) neurons for four network settings (see markers) taken from the bifurcation diagram. $N_{SOM} = N_{VIP} = 5$. SOM and VIP neurons were stimulated with an input consisting of i) a constant component of $25/s$ and ii) individual noise drawn at each

time t from a Gaussian distribution with zero mean and SD of $1/s$.
(PDF)

S6 Fig. The full microcircuit with excitatory PCs and inhibitory PV, SOM and VIP neurons shows the same phenomena as the reduced interneuron network. (A) PCs in the full microcircuit (left) exhibit a steeper firing rate slope with increasing mutual inhibition strength ($\hat{w} = 0.7$ and 0.9), increasing short-term facilitation (STF) ($U_s = 0.4$ and 0.25, $\tau_f = 200$ ms), but a reduced slope for increasing recurrence strength ($\hat{w}_r = 0$ and 0.3) and adaptation ($b = 0.2$ and 0.5, $\tau_a = 100$ ms). **(B)** With adaptation, the frequency response analysis reveals a frequency-selective amplification. **(C)** Mean SOM-SOM neuron correlation is more sensitive to increasing recurrence strength than to adaptation strength (right). Parameter (B–C): Mutual inhibition strength $\hat{w} = 0.8$.
(PDF)

S7 Fig. WTA between SOM and VIP neurons causes hysteresis in the reduced interneuron network and full microcircuit. (A) Example phase planes (top) for three distinct values of the modulatory input (cf. bottom). The intersection points of SOM- (blue) and VIP-nullcline (green) correspond to the fixed points that are either stable (filled circle) or unstable (open circle). The vector field shows the direction and strength of flow. In a WTA regime, the network exhibits bistability for a range of modulatory input values, leading to hysteresis (bottom). **(B)** Same as above for the full microcircuit. PC rate exhibits two stable states for a range of modulatory inputs. The steady-state activity depends on the initial state. Parameter (A–B): Mutual inhibition strength $\hat{w} = 1.05$.
(PDF)

S1 Appendix. Mathematical analysis of the SOM-VIP motif. Mathematical analysis of a simplified model that comprises only SOM and VIP cell populations either with recurrent connections among both SOM and VIP neurons or adaptation. The derivations provide analytical conditions for the parameter boundaries between different computational states of the SOM-VIP motif. Approximations for these boundaries for the nonlinear case that includes short-term plasticity are also provided.
(PDF)

Acknowledgments

We are grateful to Laura Bella Naumann and Filip Vercruysse for a critical reading of the manuscript.

Author Contributions

Conceptualization: Loreen Hertäg, Henning Sprekeler.

Data curation: Loreen Hertäg.

Formal analysis: Loreen Hertäg, Henning Sprekeler.

Funding acquisition: Henning Sprekeler.

Investigation: Loreen Hertäg.

Methodology: Loreen Hertäg, Henning Sprekeler.

Project administration: Henning Sprekeler.

Resources: Henning Sprekeler.

Software: Loreen Hertäg.

Supervision: Henning Sprekeler.

Validation: Loreen Hertäg, Henning Sprekeler.

Visualization: Loreen Hertäg.

Writing – original draft: Loreen Hertäg, Henning Sprekeler.

Writing – review & editing: Loreen Hertäg, Henning Sprekeler.

References

1. Isaacson JS, Scanziani M. How inhibition shapes cortical activity. Neuron. 2011; 72(2):231–243. https://doi.org/10.1016/j.neuron.2011.09.027 PMID: 22017986
2. Marín O. Interneuron dysfunction in psychiatric disorders. Nature reviews Neuroscience. 2012; 13(2):107–119. https://doi.org/10.1038/nrn3155 PMID: 22251963
3. Tremblay R, Lee S, Rudy B. GABAergic interneurons in the neocortex: from cellular properties to circuits. Neuron. 2016; 91(2):260–292. https://doi.org/10.1016/j.neuron.2016.06.033 PMID: 27477017
4. Meyer HS, Schwarz D, Wimmer VC, Schmitt AC, Kerr JN, Sakmann B, et al. Inhibitory interneurons in a cortical column form hot zones of inhibition in layers 2 and 5A. Proceedings of the National Academy of Sciences. 2011; 108(40):16807–16812. https://doi.org/10.1073/pnas.1113648108
5. Gentet LJ. Functional diversity of supragranular GABAergic neurons in the barrel cortex. Frontiers in neural circuits. 2012; 6:52. https://doi.org/10.3389/fncir.2012.00052 PMID: 22912602
6. Wamsley B, Fishell G. Genetic and activity-dependent mechanisms underlying interneuron diversity. Nature Reviews Neuroscience. 2017; p.299–309. https://doi.org/10.1038/nrn.2017.30 PMID: 28381833
7. Adesnik H, Bruns W, Taniguchi H, Huang ZJ, Scanziani M. A neural circuit for spatial summation in visual cortex. Nature. 2012; 490(7419):226. https://doi.org/10.1038/nature11526 PMID: 23060193
8. Kvitsiani D, Ranade S, Hangya B, Taniguchi H, Huang J, Kepecs A. Distinct behavioural and network correlates of two interneuron types in prefrontal cortex. Nature. 2013; 498(7454):363–366. https://doi.org/10.1038/nature12176 PMID: 23708967
9. Hangya B, Pi HJ, Kvitsiani D, Ranade SP, Kepecs A. From circuit motifs to computations: mapping the behavioral repertoire of cortical interneurons. Current opinion in neurobiology. 2014; 26:117–124. https://doi.org/10.1016/j.conb.2014.01.007 PMID: 24508565
10. Kepecs A, Fishell G. Interneuron Cell Types: Fit to form and formed to fit. Nature. 2014; 505(7483):318–326. https://doi.org/10.1038/nature12983 PMID: 24429630
11. Rudy B, Fishell G, Lee S, Hjerling-Leffler J. Three groups of interneurons account for nearly 100% of neocortical GABAergic neurons. Developmental neurobiology. 2011; 71(1):45–61. https://doi.org/10.1002/dneu.20853 PMID: 21154909
12. Avermann M, Tomm C, Mateo C, Gerstner W, Petersen CC. Microcircuits of excitatory and inhibitory neurons in layer 2/3 of mouse barrel cortex. Journal of neurophysiology. 2012; 107(11):3116–3134. https://doi.org/10.1152/jn.00917.2011 PMID: 22402650
13. Pfeffer CK, Xue M, He M, Huang ZJ, Scanziani M. Inhibition of inhibition in visual cortex: the logic of connections between molecularly distinct interneurons. Nature neuroscience. 2013; 16(8):1068–1076. https://doi.org/10.1038/nn.3446 PMID: 23817549
14. Hu H, Gan J, Jonas P. Fast-spiking, parvalbumin+ GABAergic interneurons: From cellular design to microcircuit function. Science. 2014; 345(6196):1255263.
15. Jiang X, Shen S, Cadwell CR, Berens P, Sinz F, Ecker AS, et al. Principles of connectivity among morphologically defined cell types in adult neocortex. Science. 2015; 350(6264):aac9462. https://doi.org/10.1126/science.aac9462 PMID: 26612957
16. Urban-Ciecko J, Barth AL. Somatostatin-expressing neurons in cortical networks. Nature Reviews Neuroscience. 2016; 17(7):401–409. https://doi.org/10.1038/nrn.2016.53 PMID: 27225074
17. Pi HJ, Hangya B, Kvitsiani D, Sanders JI, Huang ZJ, Kepecs A. Cortical interneurons that specialize in disinhibitory control. Nature. 2013; 503(7477):521. https://doi.org/10.1038/nature12676 PMID: 24097352
18. Fu Y, Tucciarone JM, Espinosa JS, Sheng N, Darcy DP, Nicoll RA, et al. A cortical circuit for gain control by behavioral state. Cell. 2014; 156(6):1139–1152. https://doi.org/10.1016/j.cell.2014.01.050 PMID: 24630718

19. Zhang S, Xu M, Kamigaki T, Do JPH, Chang WC, Jenvay S, et al. Long-range and local circuits for top-down modulation of visual cortex processing. Science. 2014; 345(6197):660–665. https://doi.org/10.1126/science.1254126 PMID: 25104383

20. Letzkus JJ, Wolff SB, Lüthi A. Disinhibition, a circuit mechanism for associative learning and memory. Neuron. 2015; 88(2):264–276. https://doi.org/10.1016/j.neuron.2015.09.024 PMID: 26494276

21. Pouille F, Scanziani M. Routing of spike series by dynamic circuits in the hippocampus. Nature. 2004; 429(6993):717–723. https://doi.org/10.1038/nature02615 PMID: 15170216

22. Felleman DJ, Van DE. Distributed hierarchical processing in the primate cerebral cortex. Cerebral cortex (New York, NY: 1991). 1991; 1(1):1–47.

23. Cauller LJ, Clancy B, Connors BW. Backward cortical projections to primary somatosensory cortex in rats extend long horizontal axons in layer I. Journal of Comparative Neurology. 1998; 390(2):297–310. https://doi.org/10.1002/(SICI)1096-9861(19980112)390:2%3C297::AID-CNE11%3E3.0.CO;2-V PMID: 9453672

24. Diamond ME. Somatosensory thalamus of the rat. In: The barrel cortex of rodents. Springer; 1995. p. 189–219. https://doi.org/10.1007/978-1-4757-9616-2_4

25. Larkum M. A cellular mechanism for cortical associations: an organizing principle for the cerebral cortex. Trends in neurosciences. 2013; 36(3):141–151. https://doi.org/10.1016/j.tins.2012.11.006 PMID: 23273272

26. Bartley AF, Huang ZJ, Huber KM, Gibson JR. Differential activity-dependent, homeostatic plasticity of two neocortical inhibitory circuits. Journal of neurophysiology. 2008; 100(4):1983–1994. https://doi.org/10.1152/jn.90635.2008 PMID: 18701752

27. Fino E, Yuste R. Dense inhibitory connectivity in neocortex. Neuron. 2011; 69(6):1188–1203. https://doi.org/10.1016/j.neuron.2011.02.025 PMID: 21435562

28. Packer AM, Yuste R. Dense, unspecific connectivity of neocortical parvalbumin-positive interneurons: a canonical microcircuit for inhibition? Journal of Neuroscience. 2011; 31(37):13260–13271. https://doi.org/10.1523/JNEUROSCI.3131-11.2011 PMID: 21917809

29. Lee S, Kruglikov I, Huang ZJ, Fishell G, Rudy B. A disinhibitory circuit mediates motor integration in the somatosensory cortex. Nature neuroscience. 2013; 16(11):1662–1670. https://doi.org/10.1038/nn.3544 PMID: 24097044

30. Jouhanneau JS, Kremkow J, Dorrn AL, Poulet JF. In vivo monosynaptic excitatory transmission between layer 2 cortical pyramidal neurons. Cell reports. 2015; 13(10):2098–2106. https://doi.org/10.1016/j.celrep.2015.11.011 PMID: 26670044

31. Pala A, Petersen CC. In vivo measurement of cell-type-specific synaptic connectivity and synaptic transmission in layer 2/3 mouse barrel cortex. Neuron. 2015; 85(1):68–75. https://doi.org/10.1016/j.neuron.2014.11.025 PMID: 25543458

32. Urban-Ciecko J, Fanselow EE, Barth AL. Neocortical somatostatin neurons reversibly silence excitatory transmission via GABAb receptors. Current Biology. 2015; 25(6):722–731. https://doi.org/10.1016/j.cub.2015.01.035 PMID: 25728691

33. Wilson HR, Cowan JD. Excitatory and inhibitory interactions in localized populations of model neurons. Biophysical journal. 1972; 12(1):1–24. https://doi.org/10.1016/S0006-3495(72)86068-5 PMID: 4332108

34. Murayama M, Pérez-Garci E, Nevian T, Bock T, Senn W, Larkum ME. Dendritic encoding of sensory stimuli controlled by deep cortical interneurons. Nature. 2009; 457(7233):1137. https://doi.org/10.1038/nature07663 PMID: 19151696

35. Xiang Z, Huguenard JR, Prince DA. Cholinergic switching within neocortical inhibitory networks. Science. 1998; 281(5379):985–988. https://doi.org/10.1126/science.281.5379.985 PMID: 9703513

36. Polack PO, Friedman J, Golshani P. Cellular mechanisms of brain state–dependent gain modulation in visual cortex. Nature neuroscience. 2013; 16(9):1331. https://doi.org/10.1038/nn.3464 PMID: 23872595

37. Wester JC, McBain CJ. Behavioral state-dependent modulation of distinct interneuron subtypes and consequences for circuit function. Current opinion in neurobiology. 2014; 29:118–125. https://doi.org/10.1016/j.conb.2014.07.007 PMID: 25058112

38. Chen N, Sugihara H, Sur M. An acetylcholine-activated microcircuit drives temporal dynamics of cortical activity. Nature neuroscience. 2015; 18(6):892–902. https://doi.org/10.1038/nn.4002 PMID: 25915477

39. Karnani MM, Jackson J, Ayzenshtat I, Tucciarone J, Manoocheri K, Snider WG, et al. Cooperative subnetworks of molecularly similar interneurons in mouse neocortex. Neuron. 2016; 90(1):86–100. https://doi.org/10.1016/j.neuron.2016.02.037 PMID: 27021171

40. Tsodyks MV, Markram H. The neural code between neocortical pyramidal neurons depends on neurotransmitter release probability. Proceedings of the National Academy of Sciences. 1997; 94(2):719–723.

41. Markram H, Wang Y, Tsodyks M. Differential signaling via the same axon of neocortical pyramidal neurons. Proceedings of the National Academy of Sciences. 1998; 95(9):5323–5328. https://doi.org/10.1073/pnas.95.9.5323

42. La Camera G, Rauch A, Thurbon D, Lüscher HR, Senn W, Fusi S. Multiple time scales of temporal response in pyramidal and fast spiking cortical neurons. Journal of neurophysiology. 2006; 96(6):3448–3464. https://doi.org/10.1152/jn.00453.2006 PMID: 16807345

43. Buzsáki G, Draguhn A. Neuronal oscillations in cortical networks. science. 2004; 304(5679):1926–1929. https://doi.org/10.1126/science.1099745 PMID: 15218136

44. Renart A, De La Rocha J, Bartho P, Hollender L, Parga N, Reyes A, et al. The asynchronous state in cortical circuits. Science. 2010; 327(5965):587–590. https://doi.org/10.1126/science.1179850 PMID: 20110507

45. Hasselmo ME. Neuromodulation and cortical function: modeling the physiological basis of behavior. Behavioural brain research. 1995; 67(1):1–27. https://doi.org/10.1016/0166-4328(94)00113-T PMID: 7748496

46. Giocomo LM, Hasselmo ME. Neuromodulation by glutamate and acetylcholine can change circuit dynamics by regulating the relative influence of afferent input and excitatory feedback. Molecular neurobiology. 2007; 36(2):184–200. https://doi.org/10.1007/s12035-007-0032-z PMID: 17952661

47. Muñoz W, Rudy B. Spatiotemporal specificity in cholinergic control of neocortical function. Current opinion in neurobiology. 2014; 26:149–160. https://doi.org/10.1016/j.conb.2014.02.015 PMID: 24637201

48. Stuart G, Spruston N. Determinants of voltage attenuation in neocortical pyramidal neuron dendrites. Journal of Neuroscience. 1998; 18(10):3501–3510. https://doi.org/10.1523/JNEUROSCI.18-10-03501.1998 PMID: 9570781

49. Williams SR, Stuart GJ. Dependence of EPSP efficacy on synapse location in neocortical pyramidal neurons. Science. 2002; 295(5561):1907–1910. https://doi.org/10.1126/science.1067903 PMID: 11884759

50. Yuste R, Gutnick MJ, Saar D, Delaney KR, Tank DW. Ca2+ accumulations in dendrites of neocortical pyramidal neurons: an apical band and evidence for two functional compartments. Neuron. 1994; 13(1):23–43. https://doi.org/10.1016/0896-6273(94)90457-X PMID: 8043278

51. Larkum ME, Zhu JJ, Sakmann B. A new cellular mechanism for coupling inputs arriving at different cortical layers. Nature. 1999; 398(6725):338. https://doi.org/10.1038/18686 PMID: 10192334

52. Larkum ME, Zhu JJ. Signaling of layer 1 and whisker-evoked Ca2+ and Na+ action potentials in distal and terminal dendrites of rat neocortical pyramidal neurons in vitro and in vivo. Journal of neuroscience. 2002; 22(16):6991–7005.

53. Larkum ME, Senn W, Lüscher HR. Top-down dendritic input increases the gain of layer 5 pyramidal neurons. Cerebral cortex. 2004; 14(10):1059–1070. https://doi.org/10.1093/cercor/bhh065 PMID: 15115747

54. Naud R, Sprekeler H. Sparse bursts optimize information transmission in a multiplexed neural code. Proceedings of the National Academy of Sciences. 2018; p. 201720995.

55. Larkum ME, Kaiser KMM, Sakmann B. Calcium electrogenesis in distal apical dendrites of layer 5 pyramidal cells at a critical frequency of back-propagating action potentials. Proceedings of the National Academy of Sciences. 1999; 96(25):14600–14604. https://doi.org/10.1073/pnas.96.25.14600

56. Attinger A, Wang B, Keller GB. Visuomotor coupling shapes the functional development of mouse visual cortex. Cell. 2017; 169(7):1291–1302. https://doi.org/10.1016/j.cell.2017.05.023 PMID: 28602353

57. Keller GB, Bonhoeffer T, Hübener M. Sensorimotor mismatch signals in primary visual cortex of the behaving mouse. Neuron. 2012; 74(5):809–815. https://doi.org/10.1016/j.neuron.2012.03.040 PMID: 22681686

58. Keller GB, Hahnloser RH. Neural processing of auditory feedback during vocal practice in a songbird. Nature. 2009; 457(7226):187. https://doi.org/10.1038/nature07467 PMID: 19005471

59. Eliades SJ, Wang X. Neural substrates of vocalization feedback monitoring in primate auditory cortex. Nature. 2008; 453(7198):1102. https://doi.org/10.1038/nature06910 PMID: 18454135

60. Wolpert DM, Diedrichsen J, Flanagan JR. Principles of sensorimotor learning. Nature Reviews Neuroscience. 2011; 12(12):739. https://doi.org/10.1038/nrn3112 PMID: 22033537

61. Wang XJ, Yang GR. A disinhibitory circuit motif and flexible information routing in the brain. Current opinion in neurobiology. 2018; 49:75–83. https://doi.org/10.1016/j.conb.2018.01.002 PMID: 29414069

62. Walker F, Möck M, Feyerabend M, Guy J, Wagener R, Schubert D, et al. Parvalbumin-and vasoactive intestinal polypeptide-expressing neocortical interneurons impose differential inhibition on Martinotti cells. Nature communications. 2016; 7:13664. https://doi.org/10.1038/ncomms13664 PMID: 27897179

63. Garcia-Junco-Clemente P, Ikrar T, Tring E, Xu X, Ringach DL, Trachtenberg JT. An inhibitory pull–push circuit in frontal cortex. Nature neuroscience. 2017; 20(3):389. https://doi.org/10.1038/nn.4483 PMID: 28114295

64. Pakan JM, Lowe SC, Dylda E, Keemink SW, Currie SP, Coutts CA, et al. Behavioral-state modulation of inhibition is context-dependent and cell type specific in mouse visual cortex. Elife. 2016; 5:e14985. https://doi.org/10.7554/eLife.14985 PMID: 27552056

65. del Molino LCG, Yang GR, Mejias JF, Wang XJ. Paradoxical response reversal of top-down modulation in cortical circuits with three interneuron types. eLife. 2017; 6:e29742. https://doi.org/10.7554/eLife.29742

66. Harris KD, Shepherd GM. The neocortical circuit: themes and variations. Nature neuroscience. 2015; 18(2):170. https://doi.org/10.1038/nn.3917 PMID: 25622573

67. Wall NR, De La Parra M, Sorokin JM, Taniguchi H, Huang ZJ, Callaway EM. Brain-wide maps of synaptic input to cortical interneurons. Journal of Neuroscience. 2016; 36(14):4000–4009. https://doi.org/10.1523/JNEUROSCI.3967-15.2016 PMID: 27053207

68. Spratling M. Cortical region interactions and the functional role of apical dendrites. Behavioral and cognitive neuroscience reviews. 2002; 1(3):219–228. https://doi.org/10.1177/1534582302001003003 PMID: 17715594

69. Rumelhart DE, Hintont GE, Williams RJ. Learning representations by back-propagating errors. Nature. 1986; 323:533–536. https://doi.org/10.1038/323533a0

70. Guerguiev J, Lillicrap TP, Richards BA. Towards deep learning with segregated dendrites. ELife. 2017; 6:e22901. https://doi.org/10.7554/eLife.22901 PMID: 29205151

71. Sacramento J, Costa RP, Bengio Y, Senn W. Dendritic error backpropagation in deep cortical microcircuits. arXiv preprint arXiv:180100062. 2017;.

72. Siegel M, Körding KP, König P. Integrating top-down and bottom-up sensory processing by somatodendritic interactions. Journal of computational neuroscience. 2000; 8(2):161–173. https://doi.org/10.1023/A:1008973215925 PMID: 10798600

73. Pascual-Leone A, Walsh V. Fast backprojections from the motion to the primary visual area necessary for visual awareness. Science. 2001; 292(5516):510–512. https://doi.org/10.1126/science.1057099 PMID: 11313497

74. Olson IR, Chun MM, Allison T. Contextual guidance of attention: Human intracranial event-related potential evidence for feedback modulation in anatomically early temporally late stages of visual processing. Brain. 2001; 124(7):1417–1425. https://doi.org/10.1093/brain/124.7.1417 PMID: 11408336

75. Rao RP, Ballard DH. Predictive coding in the visual cortex: a functional interpretation of some extra-classical receptive-field effects. Nature neuroscience. 1999; 2(1):79. https://doi.org/10.1038/4580 PMID: 10195184

76. Yang GR, Murray JD, Wang XJ. A dendritic disinhibitory circuit mechanism for pathway-specific gating. Nature communications. 2016; 7:12815. https://doi.org/10.1038/ncomms12815 PMID: 27649374

77. Gidon A, Segev I. Principles governing the operation of synaptic inhibition in dendrites. Neuron. 2012; 75(2):330–341. https://doi.org/10.1016/j.neuron.2012.05.015 PMID: 22841317

78. Jadi M, Polsky A, Schiller J, Mel BW. Location-dependent effects of inhibition on local spiking in pyramidal neuron dendrites. PLoS computational biology. 2012; 8(6):e1002550. https://doi.org/10.1371/journal.pcbi.1002550 PMID: 22719240

79. Wilmes KA, Sprekeler H, Schreiber S. Inhibition as a binary switch for excitatory plasticity in pyramidal neurons. PLoS computational biology. 2016; 12(3):e1004768. https://doi.org/10.1371/journal.pcbi.1004768 PMID: 27003565

80. Hayut I, Fanselow EE, Connors BW, Golomb D. LTS and FS inhibitory interneurons, short-term synaptic plasticity, and cortical circuit dynamics. PLoS computational biology. 2011; 7(10):e1002248. https://doi.org/10.1371/journal.pcbi.1002248 PMID: 22046121

81. Litwin-Kumar A, Rosenbaum R, Doiron B. Inhibitory stabilization and visual coding in cortical circuits with multiple interneuron subtypes. Journal of neurophysiology. 2016; 115(3):1399–1409. https://doi.org/10.1152/jn.00732.2015 PMID: 26740531

82. El-Boustani S, Sur M. Response-dependent dynamics of cell-specific inhibition in cortical networks in vivo. Nature communications. 2014; 5:5689. https://doi.org/10.1038/ncomms6689 PMID: 25504329

83. Lee JH, Mihalas S. Visual processing mode switching regulated by VIP cells. Scientific Reports. 2017; 7(1):1843. https://doi.org/10.1038/s41598-017-01830-0 PMID: 28500299